Catena 223 (2023) 106946

Contents lists available at ScienceDirect

Catena

journal homepage: www.elsevier.com/locate/catena

Vegetation-landslide nexus and topographic changes post the 2004 Mw 6.6 Chuetsu earthquake

Zilin Xiang [a], Jie Dou [a,b,*], Ali P. Yunus [c], Lele Zhang [a], Xiekang Wang [b], Wanqi Luo [a]

[a] Badong National Observation and Research Station of Geohazards, China University of Geosciences, Wuhan 430074, China
[b] State Key Laboratory of Hydraulics and Mountain River Engineering, Sichuan University, Chengdu 610065, China
[c] Department of Earth and Environmental Sciences, Indian Institute of Science Education and Research Mohali, Punjab 140 306, India

ARTICLE INFO

Keywords:
Chuetsu earthquake
LiDAR DEM
Landslide behavior
Vegetation recovery
Post-seismic landslide evolution

ABSTRACT

Ground shaking on steep slopes often triggers numerous landslides, which dramatically modify the landscape and have long-term effects on vegetation dynamics. However, we still have a limited understanding of the quantitative topographic evolution and the duration of post-seismic impacts on the landscapes due to the lack of long-term consistent observation, especially in low-elevation mountain regions. To address this issue, we used high-resolution pre-and post-earthquake DEMs to investigate topographic changes, as well as multi-period and multi-scale remote sensing images to analyze the post-seismic landslides and vegetation recovery in the sites affected by the Mw 6.6 2004 Chuetsu earthquake, Japan. Using a vegetation recovery rate (VRR) time series from 2004 to 2021, we examined the decaying tendency of post-seismic landslide activities and predicted the vegetation recovery rate. Our findings indicate that the Chuetsu earthquake mostly steepens and roughens the terrain in low-elevation areas. The changes to slope aspects are associated with coseismic lateral displacement. The vegetation damage area accounted for 87.98 % of the entire area after the earthquake, and the VRR reaches 85.55 % by June 2021. The number of active landslides decreased to 14.45 % after 15 years. Meanwhile, we predict that vegetation recovery areas will be restored to pre-earthquake levels in 2024, and the landslide activity rate will decrease by less than 1 % in 2026, indicating a stable hillslope devoid of debris flows in the future.

1. Introduction

Major seismic activity in mountainous ranges can set off a series of geological disasters such as ground subsidence, soil liquefaction, surface deformation, and landslides, with the latter being the most frequent (Dou et al., 2019; Dou et al., 2020; Gorum et al., 2013; Roback et al., 2018; Shafique, 2020; Shao et al., 2022; Xiong et al., 2022; Zhang et al., 2021). For example, the 1999 Mw 7.6 Chi-Chi earthquake (Shou et al., 2011), the 2008 Mw 7.9 Wenchuan earthquake (Chen et al., 2020), the 2010 Mw Haiti earthquake (Gorum et al., 2013), the 2013 Mw 7.0 Lushan earthquake (Zhao et al., 2020b), the 2015 Mw 7.6 Gorkha earthquake (Pandey et al., 2022), and the 2018 Mw 6.6 Hokkaido earthquake (Zhao et al., 2020a), all triggered thousands of coseismic landslides in the areas of maximum seismic intensity. It is estimated that these coseismic landslides lead to significant casualties and severe infrastructure destruction. In addition, the seismic shaking causes a large volume of unconsolidated material produced from the source area to accumulate in channels or on hillslopes, significantly modifying the landscape regionally and severely destroying the vegetation (Shen et al., 2020; Tang et al., 2015; Xu et al., 2016; Yunus et al., 2020, Zhang et al., 2021). Furthermore, the risk of post-seismic activity in tectonically active areas can persist for long periods and subsequently normalize gradually, but it takes years or even decades (Hovius et al., 2011; Huang and Fan, 2013; Huang and Li, 2014; Lin et al., 2006; Shafique, 2020; Yang et al., 2017; Zhao et al., 2021). Therefore, focused research efforts should be conducted to investigate the topographic changes, detect the landslide activity, and track the vegetation dynamics over a long time after the earthquake, which can provide critical guidance for post-earthquake triggered geological disaster prevention and mitigation (Lei et al., 2021; Shafique, 2020).

Thrust earthquakes not only lead to surface uplift and mountain building but also generate massive amounts of loose debris from earthquake-induced landslides (EQIL) deposited on hillslopes, which can considerably modify the features of the original landscape (Cui et al., 2012; Hovius et al., 1997; Lei et al., 2021; Parker et al., 2011; Zhao et al., 2021; Keefer, 1994). Recently, high-resolution and multi-period

* Corresponding author at: Badong National Observation and Research Station of Geohazards, China University of Geosciences, Wuhan 430074, China.
E-mail address: doujie@cug.edu.cn (J. Dou).

https://doi.org/10.1016/j.catena.2023.106946
Received 4 October 2022; Received in revised form 16 December 2022; Accepted 10 January 2023
Available online 20 January 2023

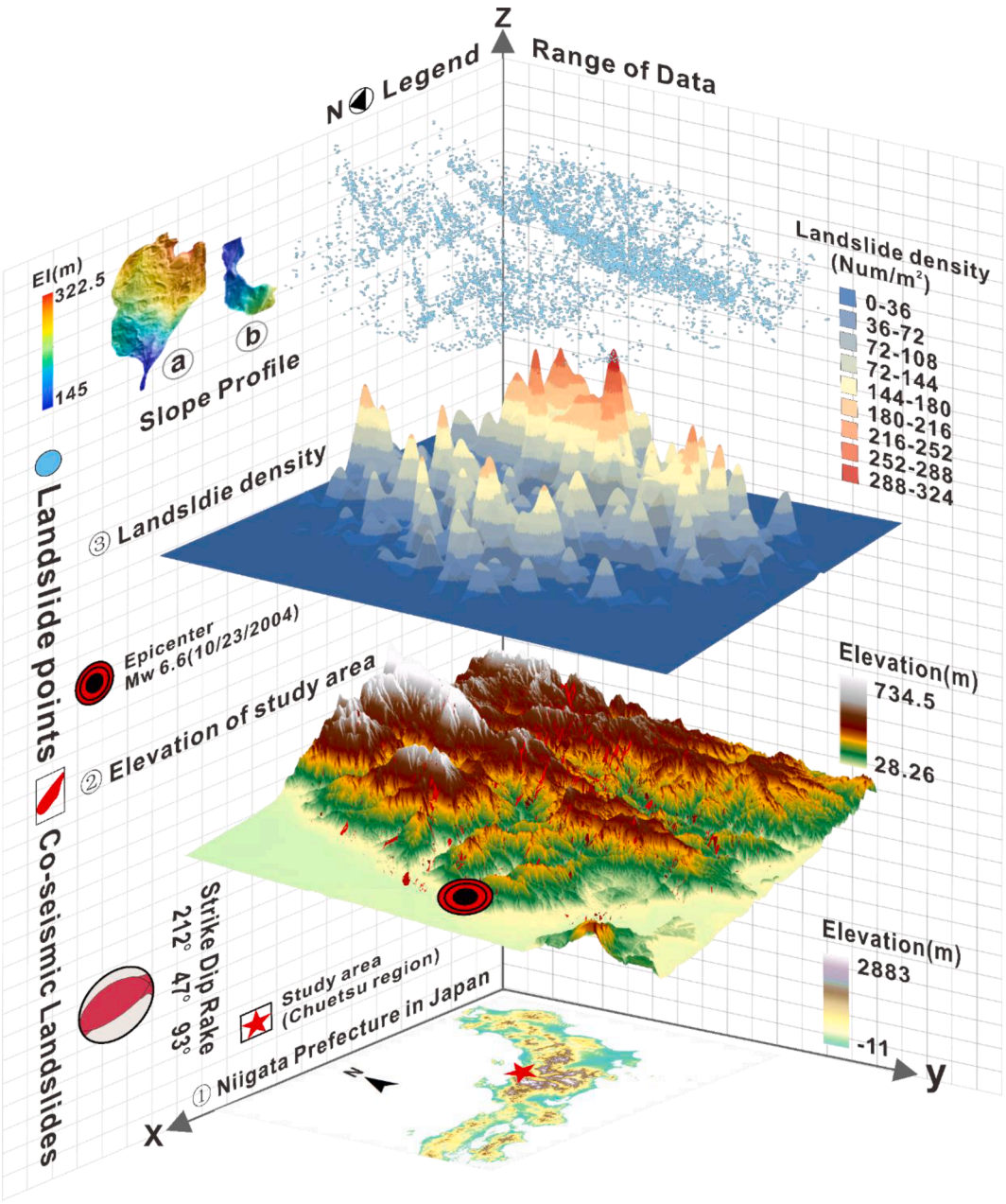

Fig. 1. Location and coseismic landslides of the study area. (a) and (b) are the largest and most typical landslides, respectively. These landslides will be used to detect topographic changes pre-and post-quake.

light detection and ranging (LiDAR) digital elevation models (DEMs) have been proven valuable in identifying changes in topographically modified areas after an earthquake (Dou et al., 2015; Maharjan et al., 2021; Ren et al., 2014; Stumpf et al., 2014; Zhou et al., 2015). For example, Ren et al. (2014) statistically analyzed the topographic changes in EQIL areas using high-resolution pre-and post-earthquake DEMs in the tectonically steep Longmen Shan region, China. It was observed that the terrain in the earthquake-affected area became smoother, with a decrease in steep slopes and ruggedness. Gorum et al. (2013) found that over 60 % of the coseismic landslides occurred on the steep mountain slopes after the 2010 Mw 7.0 Haiti earthquake. Similarly, approximately 90 % of the coseismic landslides induced by the Chi-Chi earthquake were concentrated on slopes with angles greater than 45 degrees (Lin et al., 2006). These cases show that slope modification and relief changes are common phenomena in earthquake-stricken sites. However, at present, such quantitative change analysis on topography is rarely recorded, owing to a lack of both pre-and post-event data availability. Additionally, post-seismic landslide activity shows a surge in the following few years and then gradually decays over time, and is associated with various components, such as intense precipitation, vegetation regrowth, hillslope erosion, etc. (Chen et al., 2022; Fan et al., 2019; Tang et al., 2019; Yunus et al., 2020). Among the several aforementioned factors, post-seismic natural revegetation is recognized as one of the most crucial contributors to the decreased landslide activity (Chen et al., 2022; Shen et al., 2020; Yang et al., 2018). This is because coseismic landslides damage the vegetation areas, and loose materials from the source areas curb its restoration (Chen et al., 2020; Fan et al., 2019; Huang and Li, 2014). Multi-period and high-resolution remote sensing images pre-and post-earthquake can be considered indicators to identify landslide activity and facilitate the assessment of the annual vegetation recovery rate (Chen et al., 2020; Chen et al., 2022; Lin et al., 2004; Yang et al., 2018; Yunus et al., 2020).

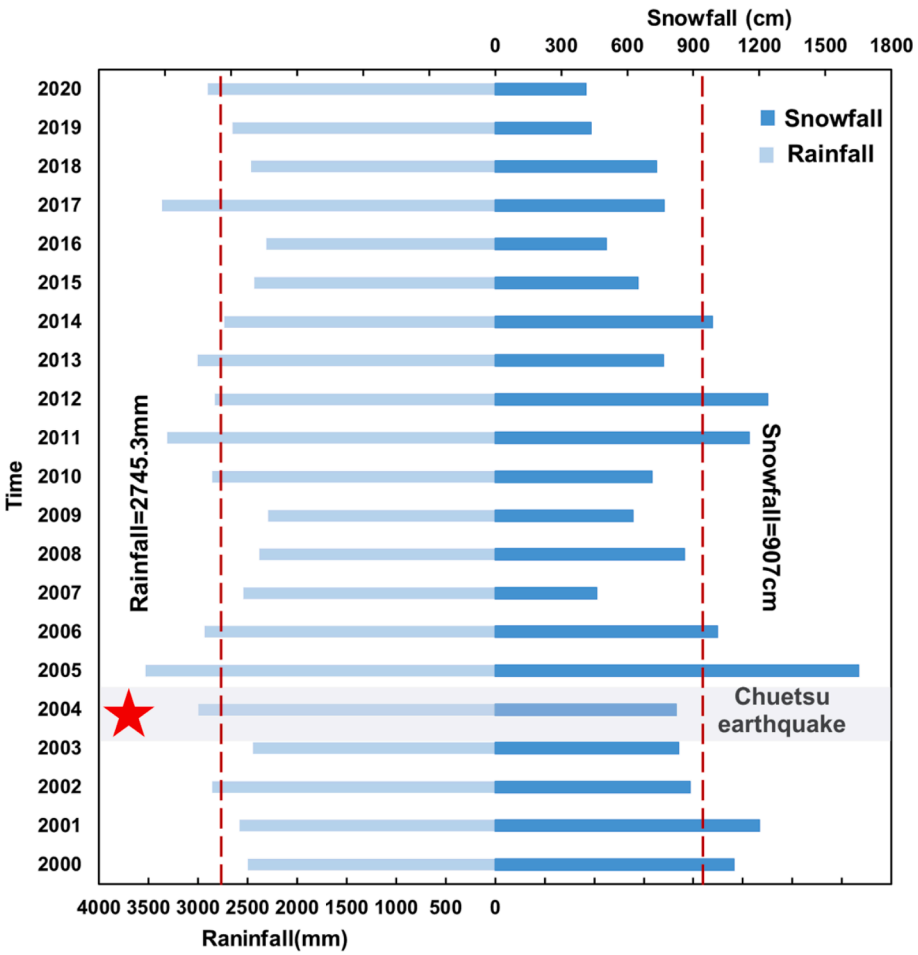

Fig. 2. Snow and rainfall statistics for the study area between 2000 and 2020 were documented at Koide and Oguni stations (source: Japan Meteorological Agency,JMA).

Many researchers have already observed increased landslide activity after earthquakes in many global earthquake cases. For example, landslide activity after the Mw 7.6 Chi-Chi earthquake and the Mw 7.9 Wenchuan earthquake persisted for several years after the main event (Hovius et al., 2011; Lin et al., 2008). It was found that post-seismic landslide activities after the Chi-Chi earthquake reduced to ~10 % in about ten years (Shou et al., 2011), and after the Mw 7.6 Kashmir earthquake, landslide activity progressively tended to be weak in around three years (Khan et al., 2013; Saba et al., 2010). Coseismic landslides after the Mw 7.9 Wenchuan earthquake are still a looming threat and have persisted for a decade (Yang et al., 2017). Using the NDVI time series from 2000 to 2018, Yunus et al. (2020) estimated that coseismic landslides would remain inactive within 18 years after the Wenchuan event. It can be noticed that the frequency of seismic activities will decrease over time with vegetation restoration.

On October 23, 2004, an Mw 6.6 earthquake occurred in the Chuetsu area of Niigata prefecture in Japan, where the maximum elevation of the epicentral area is 765 m (Lei et al., 2021). This earthquake was followed by severe aftershocks and caused thousands of coseismic landslides (Bandara and Ohtsuka, 2017). The seismic shaking can generate a large amount of unconsolidated materials, and then rapidly slide downward due to intense precipitation (Bandara and Ohtsuka, 2017; Wang et al., 2007). The sediments at the bottom of the valley were probably mobilized due to saturation and liquefaction (Valagussa et al., 2019; Wang et al., 2007), significantly reshaping the landscape in the earthquake-affected area. In the years following the Chuetsu earthquake, vegetation regrowth may enhance the soil shear and tensile strength, and alter the hydrological responses to reinforce the stabilization of slopes (Shen et al., 2020; Wang et al., 2021; Zhu and Zhang, 2019; Zou et al., 2020). Previous studies have found that the vegetation recovery function can be used as an effective proxy for assessing landslide activity and topographic stabilization (Mondini et al., 2011; Shen et al., 2020; Yang et al., 2018). As a consequence, it is evident that there is a strong connection between topographic changes and vegetation dynamics in the seismically affected areas.

Nevertheless, only a few efforts have been made to quantitatively investigate landscape evolution after seismic shaking in low-elevation mountain regions. Meanwhile, the post-seismic landslide activity and long-term revegetation in the Chuetsu region are scarcely reported. To fill this knowledge gap, this study aims to quantify the topographic changes in low-elevation areas using 2 m and 10 m high-resolution DEM and monitor the long-term regrowth of vegetation from 2003 to 2021 for the first time. The detailed objectives are as follows: i) quantify topographic changes by comparing the relief, slope angle, roughness, and slope aspect in low-elevation areas; ii) track the long-term post-seismic landslide activity and analyze the regrowth of vegetation coupling 18 years for the first time in this region; and iii) discuss the spatial distribution of post-seismic landslides with analysis to global scenarios and forecast the recovery period in earthquake-affected sites.

2. Case study

The disastrous earthquake with a moment magnitude of 6.6 struck Niigata Prefecture, Japan, in 2004 and caused numerous landslides and slope failures in the Chuetsu region (Fig. 1). The epicentral area of the main shock was located at 37°17.4′N, 138°52.2′E, with a depth of 13 km

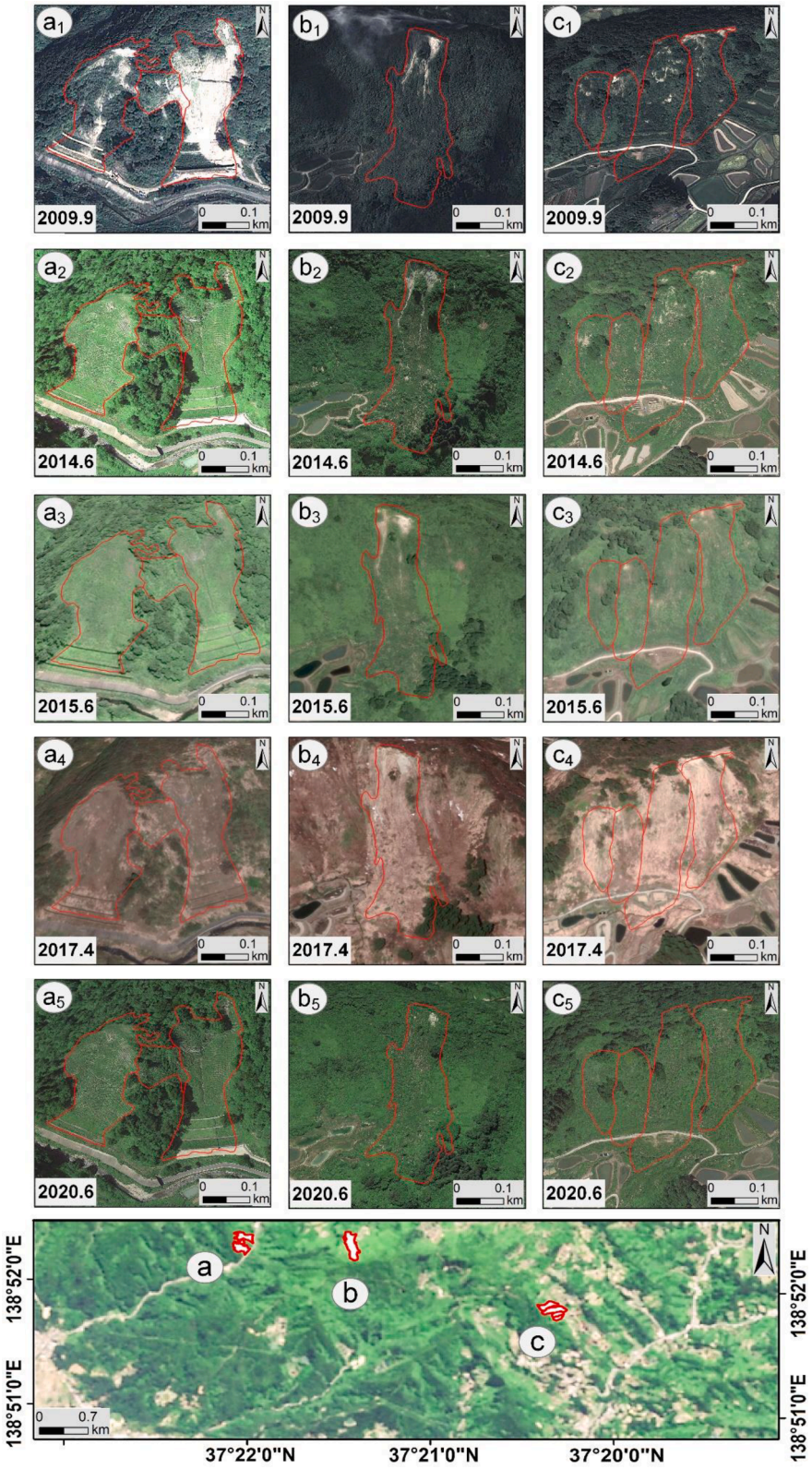

Fig. 3. Schema of interpretation of landslides and evolution characteristics of landslides after the Chuetsu earthquake for three study areas (a, b, c).

(Bandara and Ohtsuka, 2017; Japan Meteorological Agency, 2004; Lei et al., 2021). The tremendous ground motion induced by the Mw 6.6 earthquake caused extensive damage in mountainous locations and sparked thousands of landslides (Chigira and Yagi, 2006; Niigata Prefectural Government, 2009). The Chuetsu earthquake killed more than 40 people, injured almost 3,000 people, and destroyed entire upland villages (Huyck et al., 2005). The National Research Institute for Earth Science and Disaster Prevention (NIED) classified seismic-induced landslides in the Chuetsu region based on the depth of the slip surface, failure type, and moving body materials (Oyagi et al., 2008). NIED distinguished the landslides into surficial slides (depth less than 1 m), shallow slides (depth between 1 m and 10 m), and deep slides (depth

Table 1
Details of the data used in this study.

Data	Acquisition time	Scale	Data source
DEM	Before 2004	10 m	Geospatial Information Authority (GSI)
Lidar DEM	After 2004	2 m	Geospatial Information Authority (GSI)
Landslide inventory	After 2004	–	National Research Institute for Earth Science and Disaster Prevention (NIED)
Landsat TM Path 108; Row 34	2003.6.9 2005.9.18 2006.8.28 2007.6.12 2008.9.2 2013.6.4 2014.5.30 2016.5.19	30 m	National Aeronautics and Space Administration (NASA) https://earthexplorer.usgs.gov/
Landsat OLI Path 108; Row 34	2017.6.15 2018.6.2 2019.5.20 2020.8.26 2021.6.1		

greater than 10 m) based on the depth of the slip surface. In the Chuetsu area, the plains are covered in thick alluvium, and the hilly areas are mostly made up of soft mudstone from Quaternary and Tertiary deposits. Mudstone, sandstone, siltstone, and alternating bands of mudstone are the main lithological types found in the Chuetsu region (Geological Survey of Japan, 2003). This region receives an average rainfall of 2,745 mm, primarily from typhoons, as well as during the summer rain and winter snow seasons. Precipitation and snowfall in 2005 were the highest in the last two decades, as shown in Fig. 2, increasing the probability of landslide occurrence.

3. Materials

3.1. Data and landslide inventory

The vast majority of the quantitative topographic investigations in this paper are based on comparisons of high-resolution pre-and post-seismic DEMs. The 10 m resolution pre-earthquake DEM with absolute vertical precision within 2.5 m was created from stereo pairs of aerial photographs and topographic maps that cover the entire study area and are issued by the Geospatial Information Authority (GSI) of Japan. The 2 m resolution DEM post-earthquake is derived from airborne LiDAR data with a point density greater than 1pt/m^2 and published by the GSI. It has a root mean square error (RMSE) of less than 0.12 m, validated by GSI. Multi-temporal DEMs are an effective tool for statistically deriving topographic changes resulting from coseismic landslides (Chang et al., 2020; Chen et al., 2006; Li et al., 2018; Stumpf et al., 2014). In previous studies, several researchers found that errors induced by the use of different DEM scales and sources are acceptable for landslide-scale topographic change (Chen et al., 2006; Ren et al., 2014). In the present study, the high-resolution DEM datasets for pre-and post-earthquake periods were obtained from different sources. As a result, we reduced the uncertainties between the pre-and post-earthquake in this study by identifying areas with no landslide activities to calculate and then reconstruct by back-slipping the horizontal differences. Based on the reconstructed DEMs, we randomly picked 77 points in the region to quantitatively verify accuracy. The elevation difference was obtained by subtracting the pre-earthquake DEM from the post-earthquake DEM. We found that the RMSE of the elevation difference in the region was 0.23 m. In contrast, the elevation changes could reach tens of meters in coseismic landslide areas, which are much larger than RMSE found for the selected area. Consequently, quantitatively investigating the topographic changes using pre-earthquake and post-earthquake DEMs is reliable.

In addition, NIED interpreted the landslide inventory map by applying high-resolution aerial photographs (Fig. 3). In this study, vegetation recovery in landslide-affected areas was monitored through the Landsat series of satellites. The primary reason we chose Landsat as a data source is the availability of their archived data in high resolution (30 m) since the event. Detailed information on data sources is shown in Table 1.

Table 2
Classification of topographic variables.

Type	Relief (m)	Slope angle (°)	Roughness
Low	0–10	0–6	0–1.1
Medium	10–20	6–25	1.1–1.3
High	>20	>25	>1.3

Remarks: the classification of topographic changes is according to the GSI (https://www.gsi.go.jp/kiban/index.html).

3.2. Topographic change detection

The DEM data from pre-and post-earthquake periods have proven valuable in investigating topographic changes and coseismic deformations in the earthquake-triggered landslide area (Chen et al., 2006; Cowgill et al., 2010; Ren et al., 2014; Stumpf et al., 2014; Zhou et al., 2015). Previous studies have demonstrated that the multi-temporal differential DEM method is useful and effective in recognizing the topographic changes induced by coseismic landslides (Chen et al., 2006; Ren et al., 2014). We collected available high-resolution DEM data for pre-and post-earthquake periods in the Chuetsu region, which allowed us to detect the topographic changes in the earthquake-affected area. Post-earthquake 2 m resolution Lidar DEM data are firstly resampled to 10 m resolution by the cubic interpolation method to match the pre-earthquake DEM data. Four influential features of landslides (relief, slope angle, aspect, and roughness) for terrain evolution have been extensively applied to statistically detect topographic changes in this study (Dearborn and Danby, 2017; Ren et al., 2014; Rumpf et al., 2018). We extracted the aforementioned topographic derivatives, incorporating the slope aspect and gradient, from both the pre-and post-event DEMs in a GIS environment. Relief represents the actual variation of altitude in a unit area concerning its local base level, or in other words, the difference in height between the highest and the lowest points. We calculated the relief from DEM by measuring the difference between the minimum and maximum elevation within 3 × 3 pixels moving window around each pixel in a GIS environment. The roughness characterizes the variability or irregularity in elevation within a spatial unit and is defined as the ratio of the surface area to the projected area of a given site. We computed the roughness of a pixel using the focal statistics of the elevation values within a 3 × 3-pixel neighborhood around it following Evans (2019). Similarly, the slope and aspect are calculated for a 3 × 3 cell neighborhood, in which slope is computed as the rate of change of the surface in the horizontal and vertical directions, and aspect is the maximum rate of change in value from each cell to its 3 × 3 neighbors. All these computations were performed in the ArcGIS 10.8 environment.

To facilitate the analysis, the relief, slope angle, and roughness of the study area are categorized into three bins: low, medium, and high (Table 2).

3.3. Time series vegetation analysis

Devastating earthquakes have extremely grave consequences for geological hazards, including the growth of debris flows and river damming, particularly the increased frequency of landslide activities (Guo et al., 2016; Yunus et al., 2020). Post-seismic landslide activities are, to an extent, affected by diverse components, such as precipitation, erosion, and vegetation dynamics. The time-series evolution of

Table 3
Types of vegetation recovery rate (VRR).

VRR Type	VRR Value
Extremely poor	<0
Poor	0–25
Medium	25–50
Good	50–75
Very good	75–100
Extremely good	>100

vegetation post-earthquake in landslide areas can infer landslide density and intensity, and the process of vegetation recovery provides the huge potential to give us a better understanding of how long geohazards post-earthquake last (Lin et al., 2006; Wang et al., 2014). One of the most crucial indicators for assessing vegetation regrowth is the normalized difference vegetation index (*NDVI*) (Rouse et al., 1974). The enhanced vegetation index (*EVI*) can correct errors in reflected light and has greater sensitivity to high-mass areas with huge levels of chlorophyll. However, *NDVI* is utilized instead of EVI in this study as a result of the former outperforming the latter in poor vegetation areas (Matsushita et al., 2007; Testa et al., 2014). *NDVI* can be obtained using Landsat reflectivity bands 3 (*RED*) and 4 (*NIR*) through Eq. (1) (Justice et al., 1985).

$$NDVI = \frac{NIR - RED}{NIR + RED} \tag{1}$$

where *NIR* is the reflectance radiated in the near-infrared waveband and *RED* is the reflectance radiated in the visible red waveband. When the *NDVI* value increases, it means there is greater vegetation restoration in the study area. We downloaded cloud-free remote sensing images of pre-earthquake (9 June 2003) and post-earthquake (the period between September 2005 and June 2021, shown in Table 1) for vegetation change analysis.

3.3.1. Estimating vegetation damage

The Vegetation Damage Area (*VDA*) as a proxy is introduced to investigate the vegetation destruction in landslide areas before analyzing the vegetation recovery to quantitatively estimate vegetation loss in coseismic landslide sites. *VDA* is defined as Eq. (2) (Lin et al., 2005).

$$VDA = \frac{NDVI_0 - NDVI_1}{NDVI_0} \mathrm{X}100 \tag{2}$$

where $VDA > 0$ means the proportion of vegetation damage area, $NDVI_0$ is the *NDVI* value of the pre-earthquake (9 June 2003), and $NDVI_1$ is the *NDVI* value of the latest period post-earthquake (18 September 2005).

3.3.2. Estimation of vegetation restoration in landslide areas

Previous studies have shown that vegetation regrowth rates are rapid at low landslide activity frequencies (Lin et al., 2005). As a result, the vegetation restoration rate (*VRR*) is utilized to evaluate vegetation recovery areas and further estimate active and inactive landslide areas. *VRR* can be expressed as Eq. (3):

$$VRR = \frac{NDVI_1 - NDVI_2}{NDVI_1 - NDVI_0} \mathrm{X}100 \tag{3}$$

where $NDVI_0$ and $NDVI_1$ are the same as those mentioned in the previous section. In this research, $NDVI_2$ is the *NDVI* value of post-earthquake Landsat images (the period between August 2006 and June 2021). For the results, we manually grouped the *VRR* values into six categories as shown in Table 3, and we noticed that the first four rows in Table 3 ($VRR < 75$) show that the vegetation recovery area ranges from poor to fractional recovery, while the types of *Very good* and

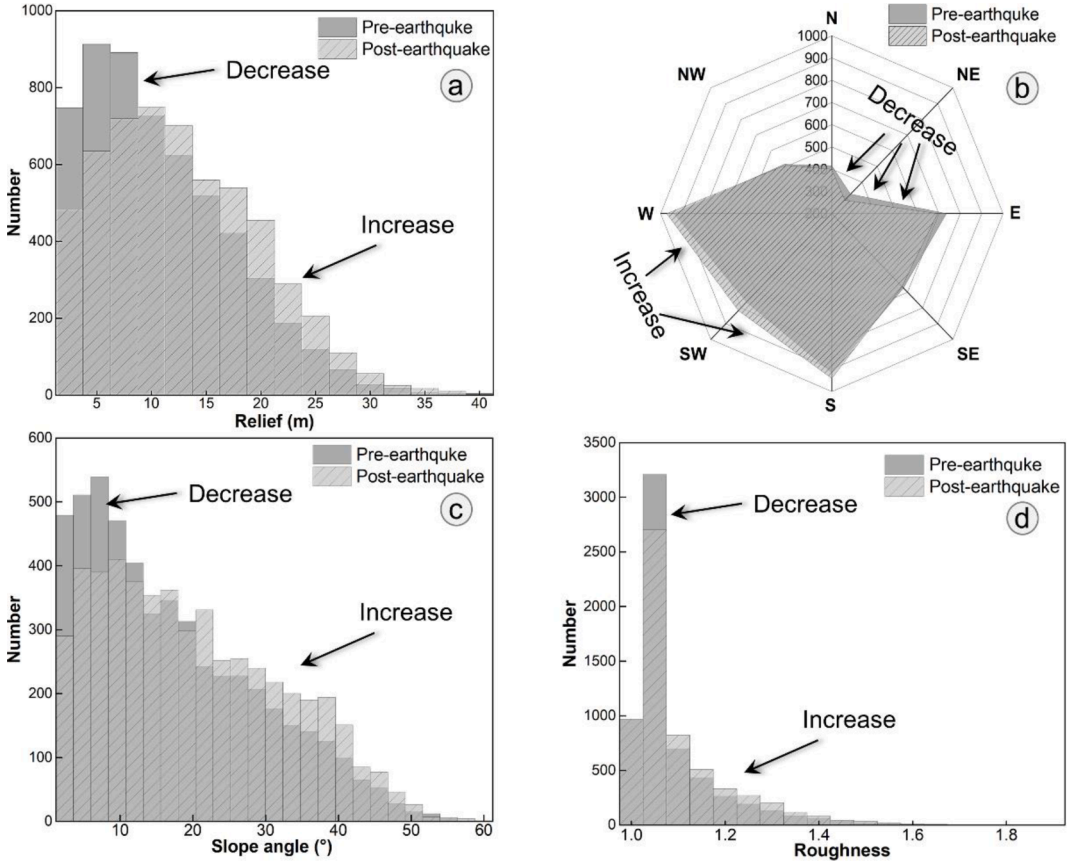

Fig. 4. Statistical comparison of the pre-and post-earthquake: (a) relief; (b) slope aspect; (c) slope angle; and (d) roughness.

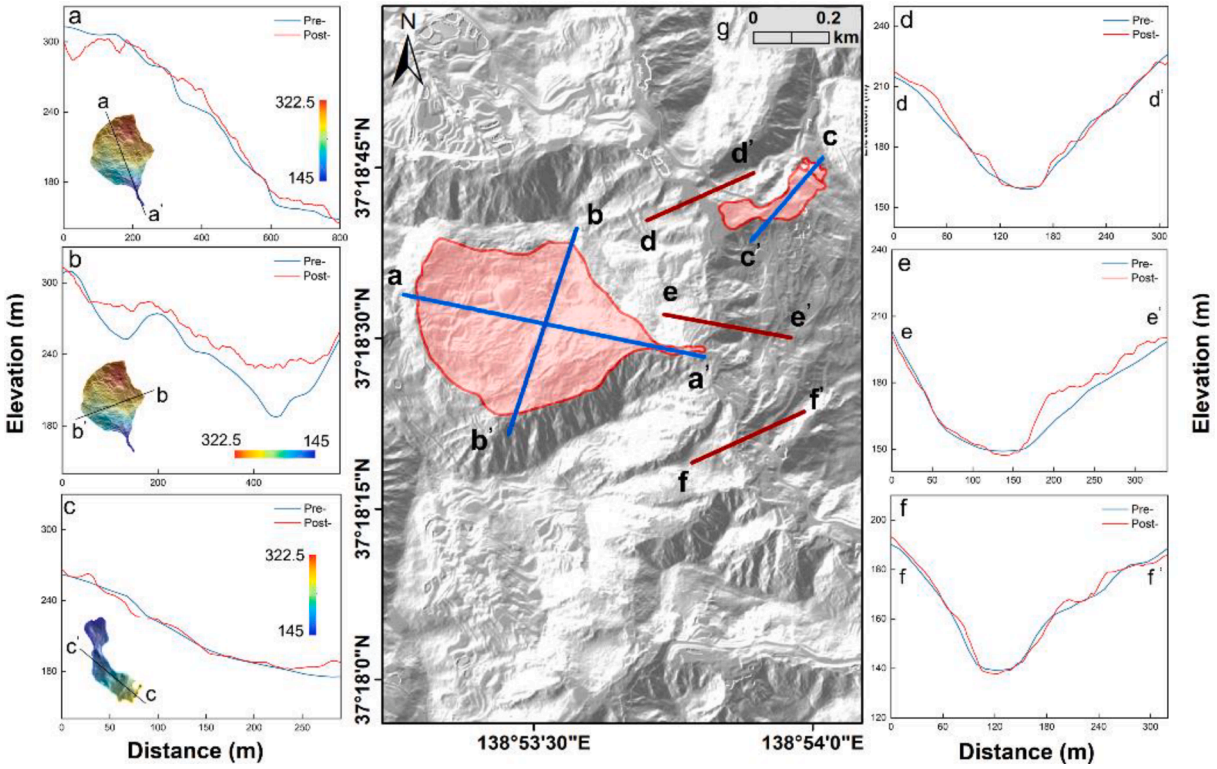

Fig. 5. (a) and (b) are the longitudinal and transverse slope profiles of the largest coseismic landslide; (c) is the slope profile of the representative landslide; (d) – (f) are the transverse cross-section profiles in (g).

Extremely good represent better vegetation restoration (Lin et al., 2005; Yunus et al., 2020). Moreover, based on the visual interpretation of *VRR* images, we categorized six *VRR* classes into two categories: active and inactive. Concretely, the *VRR* levels between *Extremely poor* and *Medium* represent poorly partial vegetation recovery and are therefore defined as active landslides, while the values in the *Good* to *Extremely good* interval are terms as inactive landslides since they represent good to excellent vegetation recovery.

4. Results

4.1. Topographic change analysis

As stated previously, a quantitative comparison of topographic characteristics pre-and post-earthquake has been proven applicable for analyzing coseismic topographic changes (Ren et al., 2014). In this work, we statistically compared the relief, slope aspect, slope angle, and roughness using resampled 10 m resolution DEMs obtained for pre-and post-earthquake time periods. The topographic evolution in coseismic landslide areas indicated a consistent increase in relief (Fig. 4a), slope angle (Fig. 4c), and roughness (Fig. 4d). Apparently, low relief areas (<10 m) showed a sharp declining trend, while those with medium and high relief areas (>10 m) increased, which was consistent with the performance of long-term earthquake-triggered landslides in Fig. 4a (Blöthe et al., 2015; Larsen and Montgomery, 2012; McPhillips et al., 2014; Roering, 2012). In particular, the 2004 Chuetsu earthquake belonged to a thrust-dominated earthquake and then altered the terrain in various forms. One possible reason might be that the increase in relief was due to the fault-related folding caused by the thrust earthquake along the N—S facing the Muikamachi-Bonchi-Seien fault (Kato et al., 2006, 2005; Okamura et al., 2007). It can be observed that the E to NW orientation and the S to E orientation had a decreasing trend, whereas west-and south-facing slopes on the west and south faces in the seismically induced areas increased (Fig. 4b). The noticed changes in the

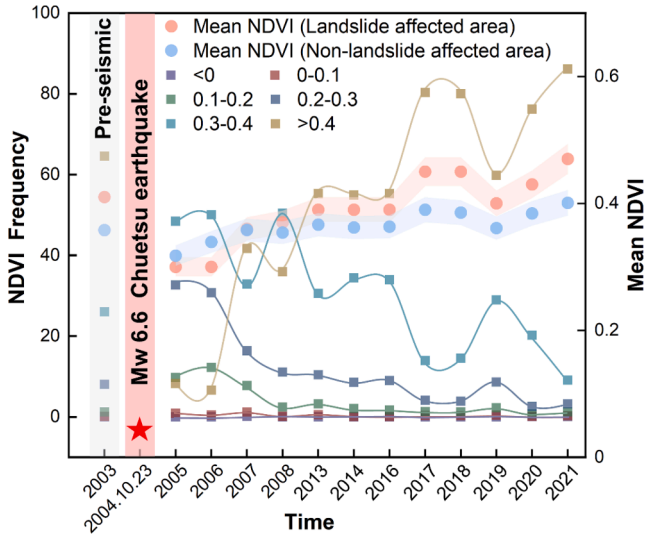

Fig. 6. Frequency distribution of NDVI in the coseismic landslide area and mean NDVI between the years 2003 and 2021.

slope aspect might be linked to the coseismic lateral displacement of the Mw 6.6 Chuetsu earthquake, which was estimated at approximately 10–20 cm (Maruyama et al., 2005). Overall, severe landslides associated with the earthquake and its aftershocks substantially steepened the landscape, as landslides caused exposure in the source areas (Fig. 4d). Meanwhile, the coseismic landslides produced a considerable amount of debris, which roughened the landscape in the Chuetsu region (Fig. 4d).

Furthermore, we chose the largest coseismic landslide area in the entire region to analyze the elevation changes caused by landslides (Fig. 5). The maximum length and width of the largest landslide were 322.5 m and 307 m, respectively (Fig. 5a-b). Meanwhile, we found that

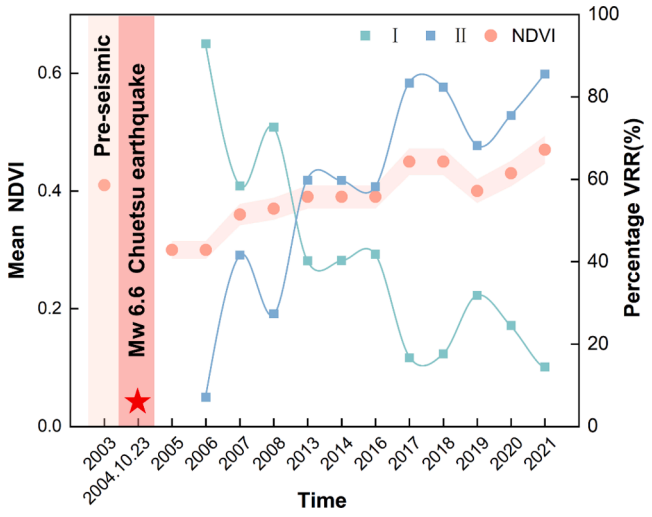

Fig. 7. Mean NDVI between the years 2003 and 2021 for the Chuetsu earthquake and percentage vegetation recovery rate for **I-II** between the years 2006 and 2021. (**I**means vegetation recovery is extremely poor, very poor, poor, and medium degree, **II** means vegetation recovery is good and very good).

transportable material accumulated ~400 m away from the source area for the largest landslide (Fig. 5a-b); however, mass material was transported to the valley at an elevation of ~260 m for small-scale landslides (Fig. 5c). The longitudinal and transverse profile analysis of the representative areas after the 2004 event reveals that the mass material scoured the valley bottom deeper; however, the overall valley width remained the same (Fig. 5d-f).

4.2. Time-series vegetation analysis

4.2.1. NDVI-frequency distribution

The NDVI frequency distribution for the 7,392 landslide polygons was examined before and after the earthquake in the Chuetsu region (Fig. 6). The NDVI value of over 0.4 accounted for more than 60 % of all landslide-induced sites before the earthquake. However, what can be seen in the graph is the dramatic decline in the NDVI value in 2005 (the first year after the earthquake). In subsequent years, NDVI values in around half of the region were maintained at 0.3–0.4, suggesting that landslide activity had further destroyed the vegetation area. Additionally, approximately 80 % of the total area had an NDVI value larger than 0.4 due to the reduction of landslide activities and an increase in revegetation in June 2017, and it peaked at 81.2 % in 2021, which indicates slope stabilization and almost full vegetation recovery in coseismic landslide areas. Similarly, the mean NDVI in landslide-affected areas has seen the same trend, where the average NDVI value recovered to its pre-earthquake level in 2017 (0.39) and hit its peak in 2021 (0.47). In addition, the mean NDVI fluctuates between 0.3 and 0.4 in areas that have not changed, i.e., have not been affected by coseismic landslides, indicating that vegetation was barely affected by landslides and remained in a stable state in these areas. Meanwhile, the tendency of the mean NDVI in non-landslide areas further illustrates the rationality of the NDVI values in landslide areas.

4.2.2. Vegetation damage area (VDA) and vegetation recovery rate (VRR)

Based on the formula described in Section 3.3.1, we found that the vegetation damage area accounted for 87.98 % (~7.088 km^2) of the entire area (~8.056 km^2) obtained through NDVI images, and landslide activities had a negligible impact on the remaining vegetative regions (~0.968 km^2). This result indicated that landslides of considerable intensity occurred throughout the earthquake-affected area, destroying extensive vegetation.

As shown in Fig. 7 and Table 4, the multi-temporal vegetation recovery rate (VRR) statistics of coseismic landslides were analyzed for nearlytwo decades. We observed that the VRR percentage statistics for areas classified as **I** dropped from 92.9 % in 2006 to roughly 10 % within 15 years, whereas those falling into the **II** class rose from less than 10 % to exceed 80 % in 2021, indicating that massive coseismic landslides and post-seismic landslides were induced by the Mw 6.6 Chuetsu earthquake from 2004 to 2006, leading to the ecological destruction of the region. From 2006 to 2021, vegetation in seismically induced areas was progressively restored, and the average NDVI value gradually returned to the pre-earthquake level, which inferred the rapid decay of landslide activities and other calamities. According to the trend, there was a sudden drop in the average NDVI value and the II categories in 2008 and 2019, where the reduction in 2008 might be related to the Mw 6.6 earthquake that struck on July 16, 2007. The 2009 event might be attributed to two possibilities. On the one hand, NDVI values are affected by contamination from neighboring areas due to their low spatial resolution (Guindin Garcia et al., 2012). On the other hand, the Chuetsu region suffered a cold snap with temperatures as low as −30 degrees, which might have contributed to the low NDVI value this year. We also performed the VRR spatial distribution for the coseismic landslides, and the representative sites for the spatial distribution map are shown in Fig. 8.

Based on the VRR and the classification criteria in Section 3.3.2, we calculate the number of active and inactive landslides in the study area. Fig. 9 illustrated that there were 5,720 active landslides and 2,897 inactive landslides in 2006. After 15 years, the number of active landslides decreased from 5,720 (66.31 %) to 1,294 (14.45 %) in 2021. Inactive landslides, on the contrary, exhibited a growing trend (from 2,897 in 2006 to 7,661 in 2021), where the trend was similar to the mean trend of the NDVI. Apparently, the increase in the number of active landslides in 2008 appears to be related to the Mw 6.6 earthquake that occurred in 2007.

Furthermore, Fig. 10 depicted the multi-period images of field investigation obtained pre-and post-earthquake. Through the analysis above, we found that there is a significant connection between reducing landslide activity and vegetation restoration. Based on model tests and

Table 4
VRR classification statistics.

Year	Extremely poor		Very Poor		Poor		Medium		Good		Very good	
	Area	%	Area	%	Area	%	Area	%	Area	%	Area	%
2003–2006	3.240	40.22	2.134	26.49	1.495	18.56	0.614	7.62	0.564	7.01	0.008	0.10
2003–2007	1.421	17.64	0.516	6.41	1.071	13.29	1.695	21.04	1.555	19.31	1.797	22.31
2003–2008	1.139	14.14	0.641	7.95	1.658	20.58	2.414	29.96	1.047	13.00	1.158	14.37
2003–2013	0.933	11.58	0.375	4.66	0.663	8.23	1.270	15.77	1.690	20.98	3.124	38.78
2003–2014	0.820	10.18	0.329	4.09	0.579	7.19	1.518	18.84	2.302	28.58	2.507	31.12
2003–2016	0.836	10.38	0.361	4.48	0.704	8.74	1.467	18.22	2.184	27.11	2.504	31.08
2003–2017	0.767	9.53	0.108	1.34	0.162	2.01	0.306	3.80	0.976	12.12	5.737	71.21
2003–2018	0.775	9.61	0.109	1.35	0.165	2.04	0.372	4.62	1.081	13.42	5.554	68.94
2003–2019	0.815	10.12	0.253	3.14	0.479	5.94	1.018	12.64	2.043	25.36	3.448	42.80
2003–2020	0.854	10.60	0.091	1.13	0.151	1.88	0.880	10.92	2.463	30.58	3.617	44.90
2003–2021	0.793	9.85	0.088	1.09	0.108	1.34	0.175	2.17	0.444	5.52	6.447	80.03

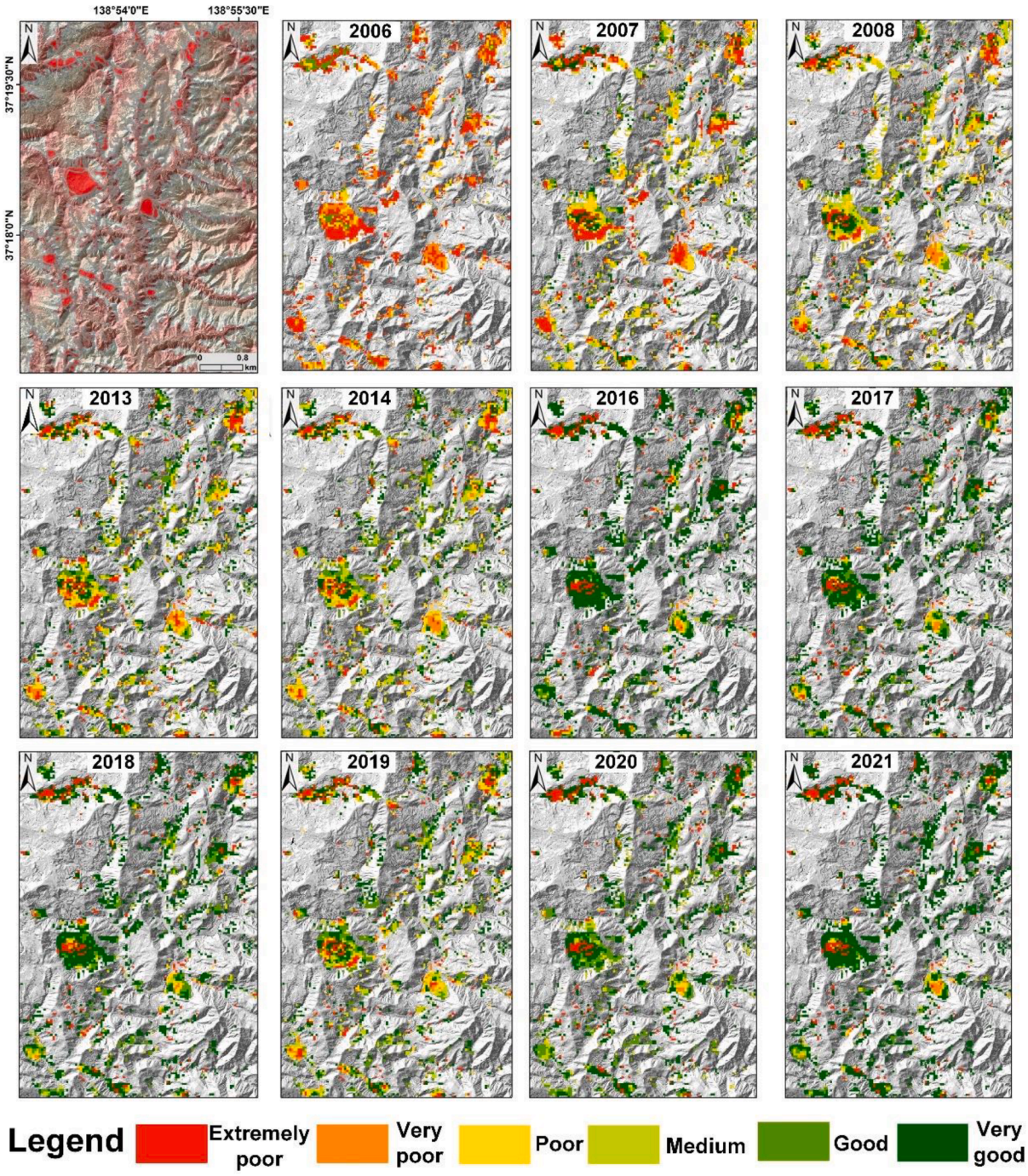

Fig. 8. Vegetation recovery rate (VRR) and the spatial distribution of vegetation recovery since 2006 in coseismic landslide areas.

field investigations, several researchers have shown that vegetation recovery could improve the stabilization of landslides since vegetation could generate additional soil shear strength and induce hydrological responses in the soil (Domènech et al., 2019; Liu et al., 2014; Shen et al., 2017; Sidle and Bogaard, 2016; Zhu and Zhang, 2019).

5. Discussion

5.1. Seismically induced landscape evolution

The high-resolution digital elevation models (DEMs) provide a robust tool to quantitatively estimate the modification of the landscape following the Mw 6.6 Chuetsu earthquake. In this study, we statistically investigated topographic changes in low-elevation areas in terms of relief, aspect, slope angle, and roughness based on pre-and post-earthquake DEMs. One of the major limitations is the inaccuracy of DEMs due to the different sources and resolutions of the pre-and post-earthquake DEMs. Nevertheless, the RMSE of the elevation difference in the region with no landslide activities was 0.23 m, indicating satisfactory performance and data quality. Consequently, detecting the topographic changes based on pre-and post-earthquake DEMs is reasonable and reliable.

In recent decades, many researchers have investigated the modification of the landscape in other earthquake cases around the world (Chigira et al., 2003; Gorum et al., 2013; Ren et al., 2014; Yang et al., 2017; Zhang et al., 2022). In the case of the Chuetsu earthquake,

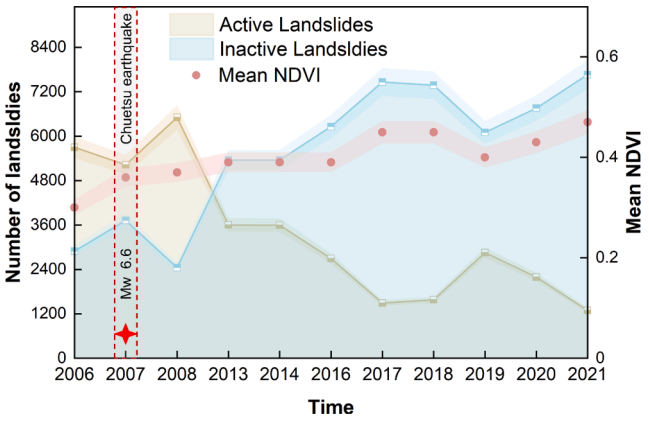

Fig. 9. The number of active and inactive landslides since 2006. Active landslides are those where vegetation has not recovered sufficiently. Meanwhile, inactive landslides are those with vegetation recovery (see Section 3.3.2).

numerous coseismic landslides were concentrated on gentle slopes (Fig. 11). We found that the slope angle and roughness increased in the seismically induced areas after the Chuetsu event, which was consistent with topographic changes after the Mw 6.6 Eastern Iburi earthquake, and the Mw 7.0 Haiti earthquake but contradicted the decreased proportion of steep slopes and roughness in the Mw 7.9 Wenchuan earthquake (Gorum et al., 2013; Ren et al., 2014). The coseismic landslides after the Chuetsu earthquake and the Eastern Iburi earthquake steepened the landscape, as they caused the exposure of steep scarps in the source areas of the landslides. The variation in slope angle and terrain ruggedness following the Haiti earthquake is related to coseismic uplifts in the epicentral region (Gorum et al., 2013). On the contrary, an increase in moderate roughness and slope angle after the Wenchuan earthquake is associated with the tectonic processes of an active fault zone (Chen and Lan, 2021; Ouimet, 2010). Furthermore, the evident alteration of slope aspects suggested that the majority of landslides are located on the north-east-facing slope in the Chuetsu region (Fig. 12). The observed changes in the slope aspect were probably attributed to the coseismic lateral displacement along the N—S facing rupture

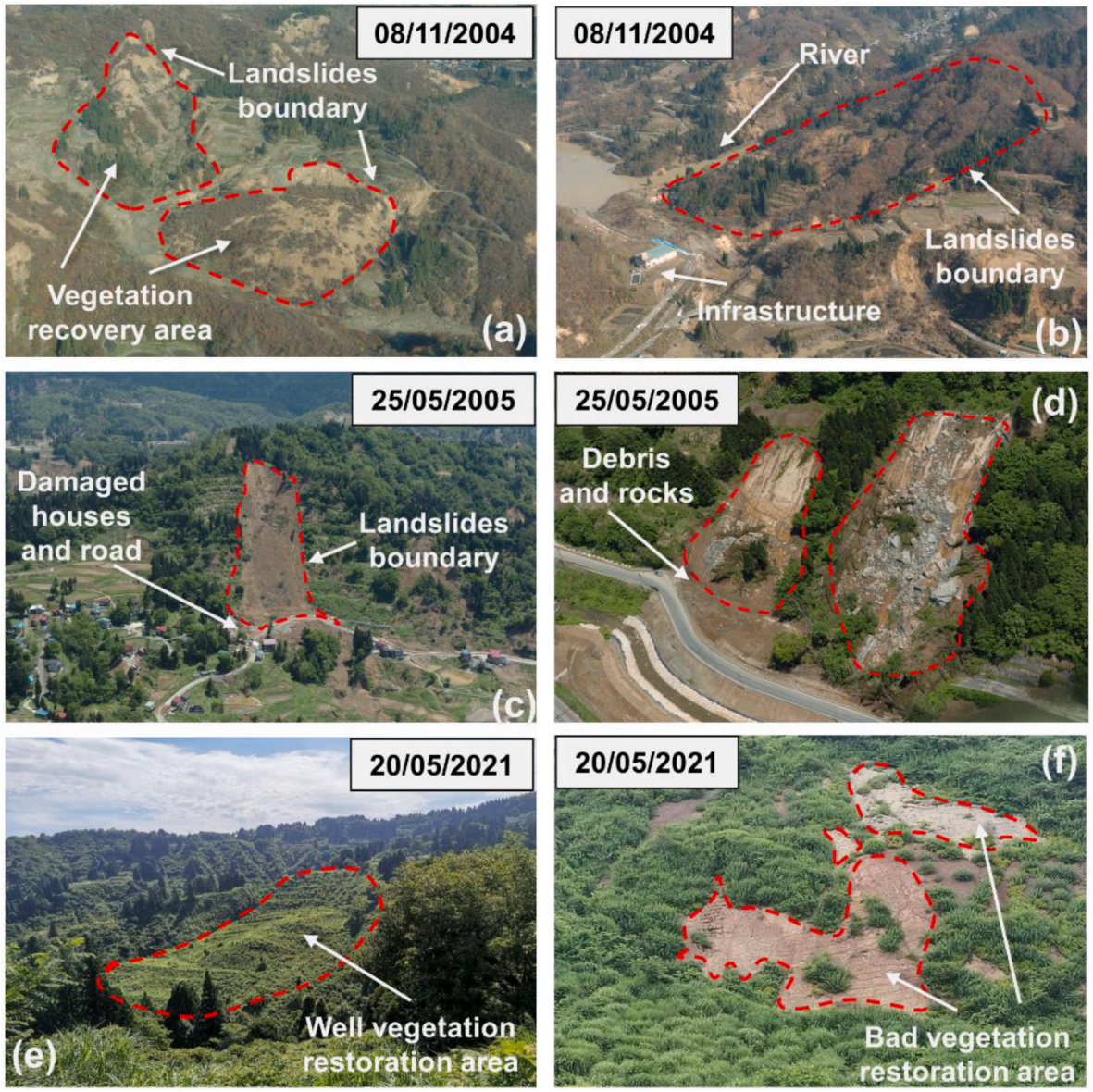

Fig. 10. Multiperiod field photos showing vegetation recovery in the landslide-affected areas of the Chuetsu region. (a)-(b) and (c)-(d) are investigated in 2004 and 2005, respectively, after the earthquake; (e) shows well-recovery vegetation in coseismic landslide areas; (f) shows areas that have not entirely recovered.

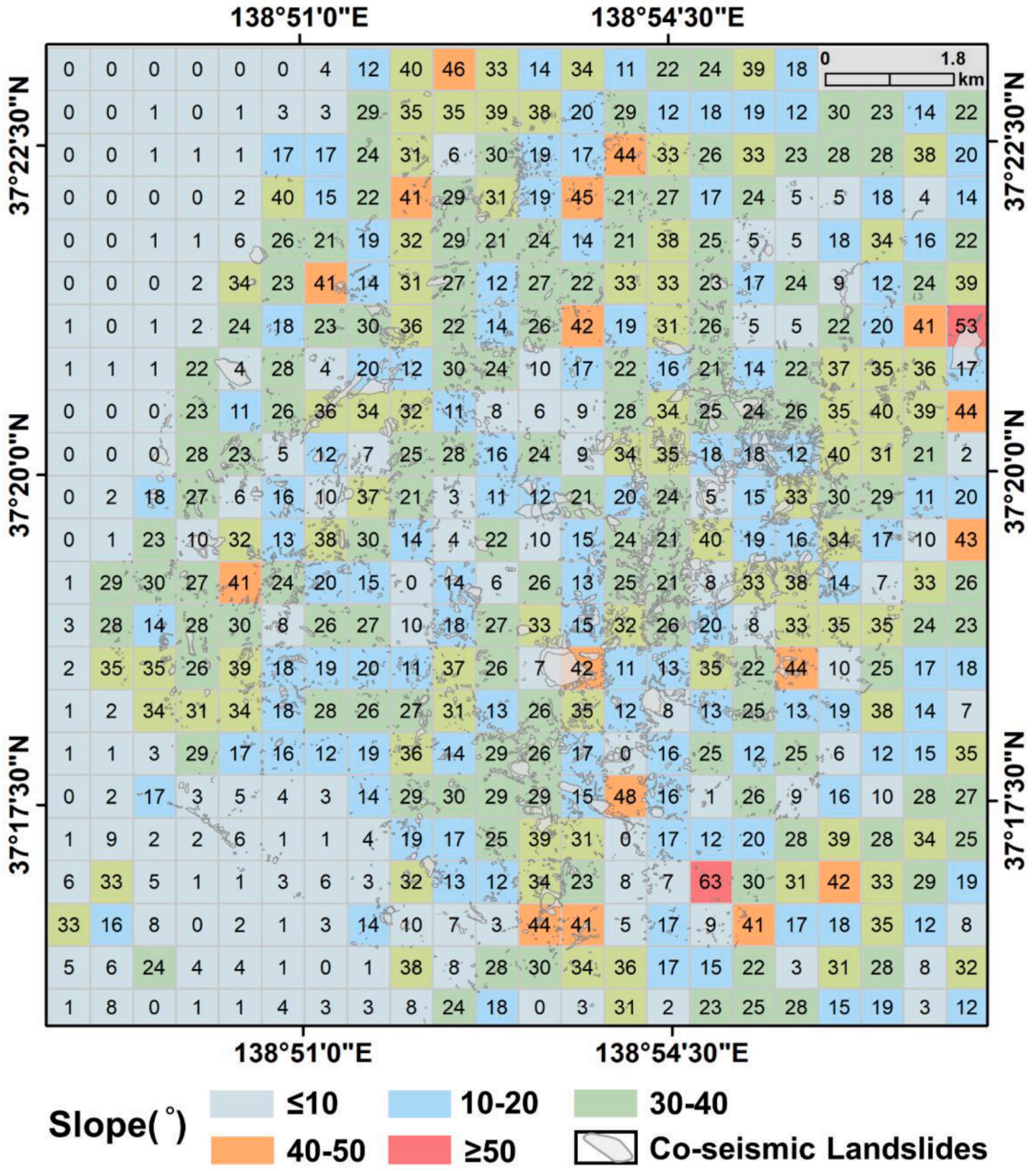

Fig. 11. Distribution and average slope of coseismic landslides induced by the Chuetsu earthquake (the number in each box represents the average slope within the cell).

(Maruyama et al., 2005). Consistent results are also found for other earthquake sites where we noticed that the seismogenic faults control the landslides in the slope aspect. According to Ren et al. (2014), the predominance of landslides on south-facing slopes showed that this aspect was more prone to coseismic failure during the Wenchuan earthquake, which might be explained by the regional compressive stress field. For the Eastern Iburi earthquake cases, the proportion of slopes in the E, SE, and S directions decreased as a result of the earthquake. This result may be connected to the SE orientation of the seismogenic source and its slip (Fan et al., 2018).

Extensive coseismic landslides occurred in low-relief areas after the Chuetsu earthquake. The alterations in relief, which could be associated with the fault-related folding caused by the thrust earthquake, were consistent with the performance of long-term earthquake-triggered landslides (Larsen and Montgomery, 2012; McPhillips et al., 2014; Roering, 2012). The average relief of coseismic landslides in Chuetsu is about 150 m, which is higher than the 2018 Hokkaido event but gentler than the 2008 Wenchuan case. Furthermore, previous studies proved that the transportable material from source sites roughened the landscape. Erosion lessened relief and eventually removed the landslides from the epicenter area, leading to a tectonic rebound at the expense of mass unloading and further modification of the terrain in the long term (Lei et al., 2021). Studies on comparisons among global earthquake cases have indicated that large topography controls the occurrence of coseismic landslides.

5.2. *Spatial distributions of landslides*

Numerous landslide inventories, including historical and fresh events, have shown that the frequency–area distribution of medium and large landslides decayed as an inverse power of the landslide area (Chang et al., 2021; Fujii, 1969; Guzzetti et al., 2002; Malamud et al.,

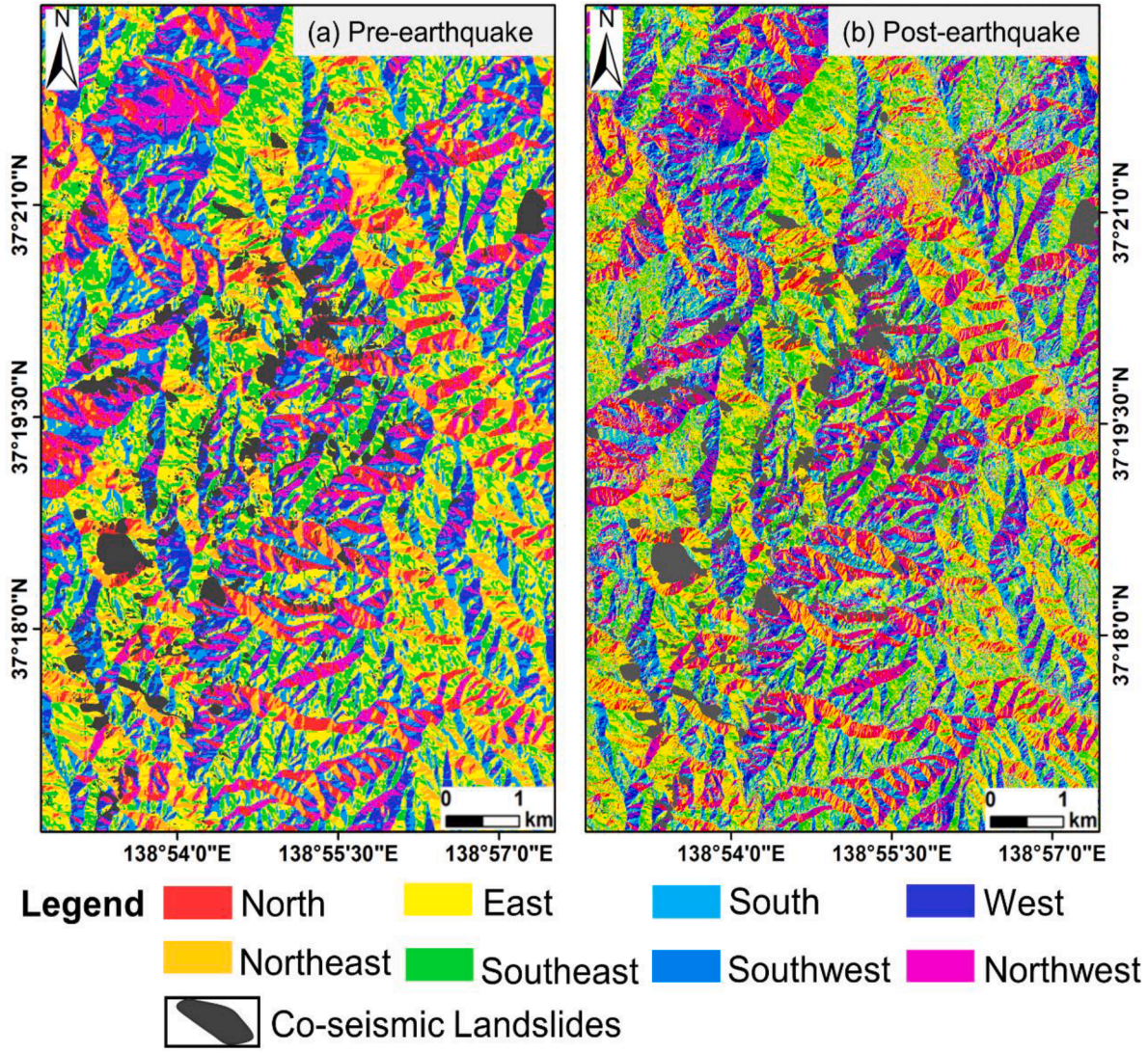

Fig. 12. Slope aspects derived from the pre- (a) and post-earthquake (b) DEMs. The maps show that the landslides occurred on north-east-facing slopes.

2004; Sugai et al., 1995). The common characteristic exists in all cases, but there are significant variances in the size and numbers. The earthquake-induced landslide inventories in the Chuetsu region were exhaustive and well documented, containing 7,392 coseismic landslides and covering 8.05 km^2 (Fig. 1). The landslide area represents 3.76 % of the total study area (213.91 km^2), with an average density throughout the area of roughly 34.55 landslides per square kilometer. Fig. 13 showed that most of the landslides were concentrated on the Muikamachi-Bonchi-Seien fault, reaching 240 Num/km^2. We plot the frequency densities of landslides triggered by the Chuetsu earthquake, shown in Fig. 14 (open squares). We noticed that the frequency densities dropped sharply as the size of landslides increased for medium and large landslide areas, while the landslide frequency-area distribution appeared to deflect for small-sized landslides (Malamud et al., 2004; Stark and Hovius, 2001; Van Den Eeckhaut et al., 2007). The rationale for the inflection is not well understood. However, part of the explanation for the rollover could be that some small landslides were excluded from the inventories (Malamud et al., 2004; Stark and Hovius, 2001). On the other hand, the rollover of the landslide size-frequency distribution is thought to be an objective physical law by several researchers (Guthrie and Evans, 2004). While no universal conclusion has been reached in the research on rollover, this quantitative analysis of the landslide area induced by an earthquake offers a valuable tool for assessing the landslide hazard.

5.3. Effects of post-seismic vegetation recovery on the decay of landslide activity

The vegetation recovery rate of the slope varied with the post-seismic landslide activities, affected by scales of denudation, degrees of hydration, and climatic conditions (Chen et al., 2020; Fan et al., 2021; Dou et al., 2022). The new landslides were revealed using high-resolution remote sensing images in four stages following the earthquake, in 2008, 2012, 2016, and 2020, respectively (Fig. 15). We found some new landslides that occur in the region. In general, 16 (0.27 km^2), 49 (0.155 km^2), 8 (0.002 km^2), and 16 (0.004 km^2) new landslides have occurred in these four years.

Vegetation recovery progressively returning to the pre-earthquake level after the earthquake is a first-order indicator of decayed post-seismic landslide activities (Pandey et al., 2022; Saito et al., 2022; Zhong et al., 2021). Several studies demonstrated that NDVI values considerably decreased after the earthquake, and then gradually rose in the following years, indicating extensive vegetation destruction caused by coseismic landslides and subsequent vegetation restoration (Amano et al., 2021; Yang et al., 2017). Likewise, NDVI fluctuations followed a similar pattern in our work. In the aftermath of the Wenchuan earthquake, the average revegetation rate was approximately 10.08 % within 4.5 years post-seismic in earthquake-affected areas, and the vegetation will return to pre-earthquake levels in 2020 (Li et al., 2016). Another

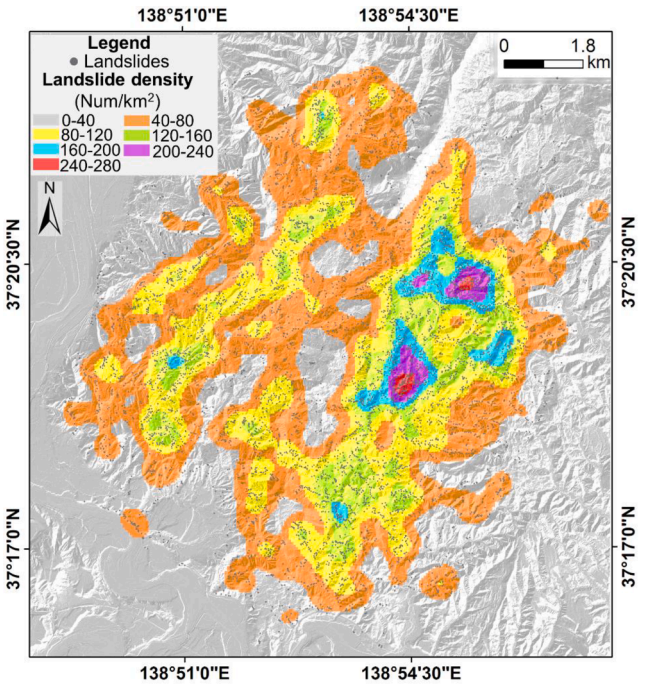

Fig. 13. The map of coseismic landslide density. Red areas represent high-density coseismic landslides, which are located close to the seismogenic faults. (For interpretation of the references to colour in this figure legend, the reader is referred to the web version of this article.)

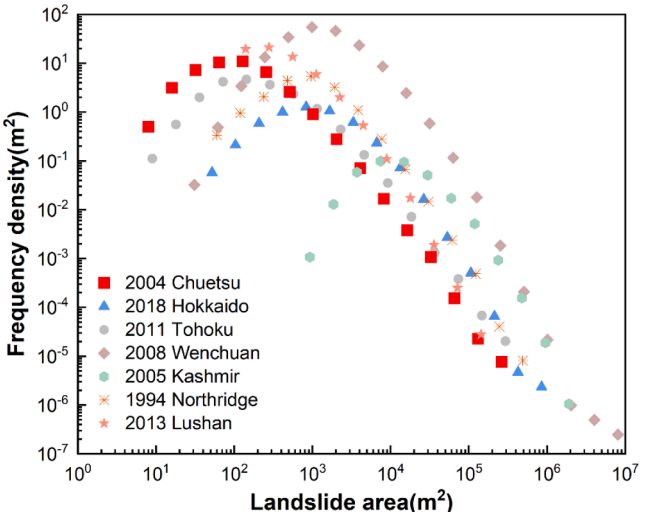

Fig. 14. Dependence of landslide frequency densities on landslide area. Probability densities are given on logarithmic axes. The red open squares represent the frequency density of the Chuetsu earthquake. (For interpretation of the references to colour in this figure legend, the reader is referred to the web version of this article.)

study tracked the vegetation evolution in the coseismic landslide areas induced by the Wenchuan earthquake and predicted that the NDVI would return to the pre-seismic level of NDVI by roughly 2025 (Yang et al., 2017). As for the Chi-Chi event that occurred in Taiwan, the vegetation in damaged areas would recover to the pre-earthquake vegetation level within seven to ten years (Lin et al., 2006; Shou et al., 2011). In this study, we evaluated the rate using the VRR approach and found that vegetation would restore pre-earthquake levels in 2024 when the vegetation area could reach 8.4 km^2 (Fig. 16).

The existence of recovered vegetation could infer that the slopes are at least temporarily stable, and this slope stability is a prerequisite for vegetation colonization (Gan et al., 2019; Huang et al., 2020; Shiels et al., 2008). In recent decades, some hypotheses on the temporal and spatial evolution of post-earthquake landslides have been proposed in other global earthquake cases. After the Wenchuan earthquake, landslide activities would return to pre-seismic conditions within two decades (Yang et al., 2017), while the recovery rate is quicker as studied by Yunus (2020). The effect of the 1999 Chi-Chi earthquake decayed to around 50 % in 1–3 years and roughly 10 % within 10 years (Shou et al., 2011). In the case of the Mw 7.9 Kanto earthquake in Japan, landslide activities persisted for approximately 40–50 years, with the most active period occurring in the first 15 years after the earthquake (Nakamura et al., 2000). In our work, we quantified changes in the activity rate based on the active landslide areas. The landslide activity rate in this work exhibited a power-law trend of decay over time (Fig. 16). The rate of landslide activity will decline by less than 1 % in 2026 if it follows this pattern after the 2004 Chuetsu earthquake, indicating that the impact of the Chuetsu earthquake on landslide activity will be almost eliminated. The decay tendency of the Chuetsu earthquake is very similar to that of the Wenchuan earthquake and the Chi-Chi earthquake (Chen et al., 2020; Liu et al., 2009). Consequently, vegetation restoration at landslide sites, on the one hand, is likely to facilitate the stabilization of slopes; even early successional plants like herbaceous species can help lessen the risk of re-sliding on landslides (Stokes et al., 2009). On the other hand, raindrops could be reduced by the canopy of restored plants, and their root systems could improve bulk soil strength (Huang et al., 2020a, b; Jiang et al., 2018; Luo et al., 2022; Sidle and Ochiai, 2006; Swanson and Dyrness, 1975). The above analysis shows that vegetation recovery in quake-affected areas is an important control component of post-earthquake landslide risk management. However, one limitation of NDVI-based vegetation analysis is that it considers even small grasslands as high vegetation recovered coseismic areas, but this cannot be true. Smaller roots in grasslands, although they prevent soil erosion, cannot be sustained when there is heavy rainfall present.

These findings improve our understanding of topographic changes in seismically induced areas and the decay patterns of landslide activity over time. Nevertheless, seasonal fluctuations of the multi-period NDVI may introduce uncertainties in computing VRR due to the dates of Landsat images. Additionally, the quantitative linkage between the stable state of slopes and vegetation recovery is an important issue for future research.

6. Conclusion

By quantitatively comparing pre-and post-earthquake high-resolution DEMs and multi-period remote sensing images from 2003 to 2021, we tracked the topographic changes and investigated the vegetation response from the viewpoint of spatial and temporal evolution following the 2004 Mw 6.6 Chuetsu earthquake. The main results are summarized below:

1) Our statistical analysis revealed that slope angle and roughness changed considerably after the 2004 Mw 6.6 Chuetsu earthquake. Detailed analysis indicates that the area of low relief decreased, whereas the areas of medium and high relief increased. The decline of slope aspects suggests that the E-to-NE orientation and the S-to-E orientation were affected by the coseismic lateral displacement, which was estimated at approximately 10–20 cm.
2) In terms of vegetation evolution, we analyzed the vegetation recovery rate in the 15 years after the Chuetsu earthquake using an NDVI time series from 2003 to 2021. The mean NDVI value of the landslide areas decreased from 0.41 to 0.30 following the earthquake and recovered to the pre-earthquake level in 2017. The vegetation damage area accounted for 87.98 % (~7.088 km^2) of the entire area (~8.056 km^2). The VRR reaches 85.55 % by June 2021. The overall vegetation recovery is good.

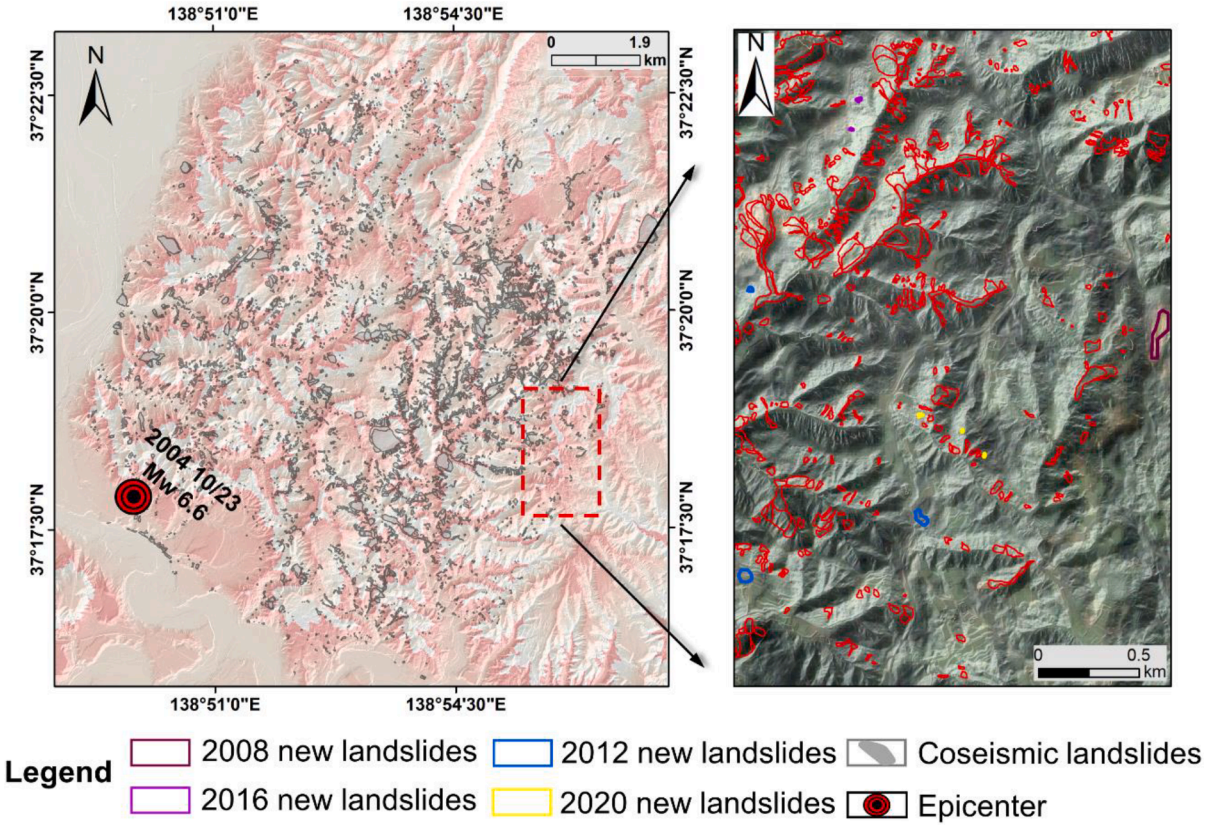

Fig. 15. New landslides in 2008, 2012, 2016, and 2020. The red dashed frame is a typical area of the new landslide. (For interpretation of the references to colour in this figure legend, the reader is referred to the web version of this article.)

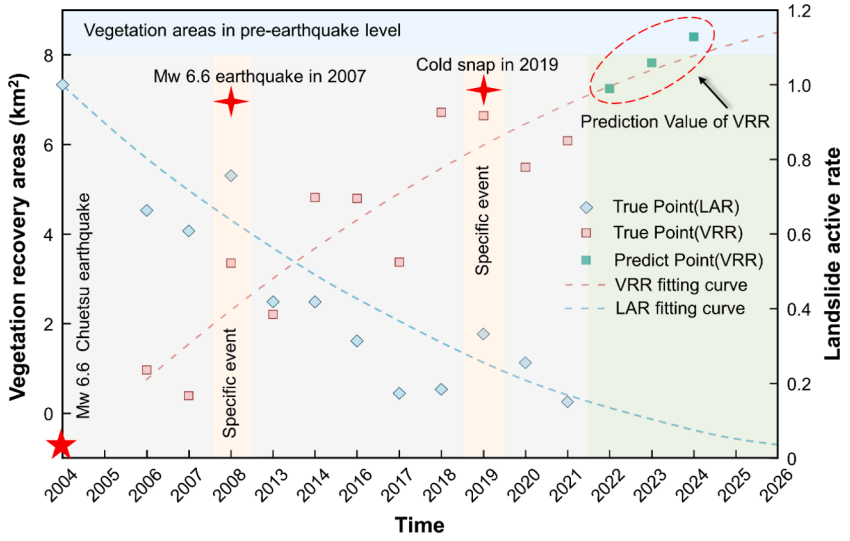

Fig. 16. The trend of the vegetation recovery area and the active rate post-earthquake in the study area. The blue line is an overall regression line of the active rate after the Chuetsu earthquake, and the red line is an overall regression line of the vegetation recovery area. Two red marks represent an Mw 6.6 earthquake in 2007 and a cold snap in 2019 respectively. (For interpretation of the references to colour in this figure legend, the reader is referred to the web version of this article.)

3) Landslides are concentrated on the Muikamachi-Bonchi-Seien fault, and the frequency densities of the landslide areas follow a power-law distribution. The vegetation recovery rate of the slope varied with the post-seismic landslide activities. The vegetation recovery area will be restored to pre-earthquake levels in 2024, and the landslide activity rate will decline by less than 1 % in 2026.

Our findings can provide insightful information for landslide hazard mitigation in the aftermath of the 2004 Mw 6.6 Chuetsu earthquake.

Data Availability Statement

The pre-earthquake digital elevation model used in this study for topographic analysis is freely available from the Geospatial Information Authority of Japan (GSI: https://www.gsi.go.jp/). Post-earthquake digital elevation models are copyrighted to Shin Engineering Company. Post-seismic landslides are mapped from Sentinel-2 images and are downloaded from https://scihub.copernicus.eu. All of the processed

data and shapefiles from this study will be available at https://10.5281/zenodo.5618609.

Declaration of Competing Interest

The authors declare that they have no known competing financial interests or personal relationships that could have appeared to influence the work reported in this paper.

Data availability

Data will be made available on request.

Acknowledgments

This research is supported by the National Natural Science Foundation of China (Major Program No. 42090054 and No. 52239006), the Natural Science Foundation of Hubei Province of China (Innovation Group Program: No. 2022CFA002), and the opening fund from the State Key Laboratory of Hydraulics and Mountain River Engineering, Sichuan University (Grant No. SKHL1903 and SKHL2003). The authors are grateful to Prof. Hiromitsu Yamagishi for providing the data and valuable discussion and comments.

References

Amano, H., Iwasaki, Y., Ichikawa, T., 2021. Identification of paddy fields using temporal NDVI changes in Minamiaso Village, Kumamoto Prefecture, Japan to estimate groundwater recharge. IOP Conf. Ser. Earth Environ. Sci. 633 https://doi.org/10.1088/1755-1315/633/1/012012.

Bandara, S., Ohtsuka, S., 2017. Spatial distribution of landslides induced by the 2004 Mid-Niigata prefecture earthquake, Japan 1877–1886. doi: 10.1007/s10346-017-0819-6.

Blöthe, J.H., Korup, O., Schwanghart, W., 2015. Large landslides lie low: excess topography in the Himalaya-Karakoram ranges. Geology 43, 523–526.

Chang, M., Cui, P., Xu, L., Zhou, Y., 2021. The spatial distribution characteristics of coseismic landslides triggered by the Ms7.0 Lushan earthquake and Ms7.0 Jiuzhaigou earthquake in southwest China. Environ. Sci. Pollut. Res. 28, 20549–20569. https://doi.org/10.1007/s11356-020-11826-5.

Chang, Z., Du, Z., Zhang, F., Huang, F., Chen, J., Li, W., Guo, Z., 2020. Landslide susceptibility prediction based on remote sensing images and GIS: comparisons of supervised and unsupervised machine learning models. Remote Sens. 12 https://doi.org/10.3390/rs12030502.

Chen, R.-F., Chang, K.-J., Angelier, J., Chan, Y.-C., Deffontaines, B., Lee, C.-T., Lin, M.-L., 2006. Topographical changes revealed by high-resolution airborne LiDAR data: The 1999 Tsaoling landslide induced by the Chi-Chi earthquake. Eng. Geol. 88, 160–172. https://doi.org/10.1016/j.enggeo.2006.09.008.

Chen, X., Lan, J., 2021. Impact of slope stability changes on landslide activity near the epicenter of the 2008 Wenchuan Ms8.0 earthquake. China. Bull. Eng. Geol. Environ. 80, 5259–5270. https://doi.org/10.1007/s10064-021-02147-z.

Chen, M., Tang, C., Xiong, J., Shi, Q.Y., Li, N., Gong, L.F., Wang, X.D., Tie, Y., 2020. The long-term evolution of landslide activity near the epicentral area of the 2008 Wenchuan earthquake in China. Geomorphology 367. https://doi.org/10.1016/j.geomorph.2020.107317.

Chen, M., Tang, C., Li, M., Xiong, J., Luo, Y., Shi, Q., Zhang, X., Tie, Y., Feng, Q., 2022. Changes of surface recovery at coseismic landslides and their driving factors in the Wenchuan earthquake-affected area. Catena 210, 105871. https://doi.org/10.1016/j.catena.2021.105871.

Chigira, M., Wang, W.N., Furuya, T., Kamai, T., 2003. Geological causes and geomorphological precursors of the Tsaoling landslide triggered by the 1999 Chi-Chi earthquake. Taiwan. Eng. Geol. 68, 259–273. https://doi.org/10.1016/S0013-7952(02)00232-6.

Chigira, M., Yagi, H., 2006. Geological and geomorphological characteristics of landslides triggered by the 2004 Mid Niigta prefecture earthquake in Japan. Eng. Geol. 82, 202–221. https://doi.org/10.1016/j.enggeo.2005.10.006.

Cowgill, E., Bernardin, T.S., Oskin, M.E., Bowles, C., Yikilmaz, M.B., Kreylos, O., Elliott, A.J., Bishop, M.S., Kellogg, L.H., 2010. Analysis of LIDAR Data during Rapid Scientific Response to the January 12, 2010 Haiti Earthquake. In: Geological Society of American Abstracts with Programs. p. 154.

Cui, P., Lin, Y.M., Chen, C., 2012. Destruction of vegetation due to geo-hazards and its environmental impacts in the Wenchuan earthquake areas. Ecol. Eng. 44, 61–69. https://doi.org/10.1016/j.ecoleng.2012.03.012.

Dearborn, K.D., Danby, R.K., 2017. Aspect and slope influence plant community composition more than elevation across forest–tundra ecotones in subarctic Canada. J. Veg. Sci. 28, 595–604.

Domènech, G., Fan, X., Scaringi, G., van Asch, T.W.J., Xu, Q., Huang, R., Hales, T.C., 2019. Modelling the role of material depletion, grain coarsening and revegetation in debris flow occurrences after the 2008 Wenchuan earthquake. Eng. Geol. https://doi.org/10.1016/j.enggeo.2019.01.010.

Dou, J., Paudel, U., Oguchi, T., Uchiyama, S., Hayakawa, Y.S., 2015. Shallow and deep-seated landslide differentiation using support vector machines: a case study of the chuetsu area. Japan. Terr. Atmos. Ocean. Sci. 29, 227–239. https://doi.org/10.3319/TAO.2014.12.02.07(EOSI).

Dou, J., Yunus, A.P., Tien Bui, D., Sahana, M., Chen, C.-W., Zhu, Z., Wang, W., Pham, B. T., 2019. Evaluating GIS-based multiple statistical models and data mining for earthquake and rainfall-induced landslide susceptibility using the LiDAR DEM. Remote Sens. 11, 638. https://doi.org/10.3390/rs11060638.

Dou, J., Yunus, A.P., Merghadi, A., Shirzadi, A., Nguyen, H., Hussain, Y., Avtar, R., Chen, Y., Pham, B.T., Yamagishi, H., 2020. Different sampling strategies for predicting landslide susceptibilities are deemed less consequential with deep learning. Sci. Total Environ. 720, 137320 https://doi.org/10.1016/j.scitotenv.2020.137320.

Dou, J., Xiang, Z., Qiang, X., Zheng, P., Wang, X., Su, A., Liu, J., Luo, W., 2022. Application and development trend of machine learning in landslide intelligent disaster prevention and mitigation. Earth Sci. https://doi.org/10.3799/dqkx.2022.419.

Evans, I.S., 2019. General Geomorphometry, Derivatives of Altitude, and Descriptive Statistics, first ed. Spatial Analysis in Geomorphology. London. doi: 10.4324/9780429273346-2.

Fan, X., Scaringi, G., Xu, Q., Zhan, W., Dai, L., Li, Y., Pei, X., Yang, Q., Huang, R., 2018. Coseismic landslides triggered by the 8th August 2017 Ms 7.0 Jiuzhaigou earthquake (Sichuan, China): factors controlling their spatial distribution and implications for the seismogenic blind fault identification. Landslides 15, 967–983. https://doi.org/10.1007/s10346-018-0960-x.

Fan, X., Scaringi, G., Korup, O., West, A.J., Westen, C.J., Tanyas, H., Hovius, N., Hales, T. C., Jibson, R.W., Allstadt, K.E., Zhang, L., Evans, S.G., Xu, C., Li, G., Pei, X., Xu, Q., Huang, R., 2019. Earthquake-induced chains of geologic hazards: patterns, mechanisms, and impacts. Rev. Geophys. 57, 421–503. https://doi.org/10.1029/2018RG000626.

Fan, X., Yunus, A.P., Scaringi, G., Catani, F., Siva Subramanian, S., Xu, Q., Huang, R., 2021. Rapidly evolving controls of landslides after a strong earthquake and implications for hazard assessments. Geophys. Res. Lett. 48, e2020GL090509 https://doi.org/10.1029/2020GL090509.

Fujii, Y., 1969. Frequency distribution of landslides caused by heavy rainfall. J. Seism. Soc. Jpn 22, 244–247.

Gan, B. rui, Yang, X. guo, Zhang, W., Zhou, J. wen, 2019. Temporal and spatial evolution of vegetation coverage in the Mianyuan river basin influenced by strong earthquake disturbance. Sci. Rep. 9, 1–14. doi: 10.1038/s41598-019-53264-5.

Gorum, T., van Westen, C.J., Korup, O., van der Meijde, M., Fan, X., van der Meer, F.D., 2013. Complex rupture mechanism and topography control symmetry of mass-wasting pattern, 2010 Haiti earthquake. Geomorphology 184, 127–138. https://doi.org/10.1016/j.geomorph.2012.11.027.

Guindin Garcia, N., Gitelson, A.A., Arkebauer, T.J., Shanahan, J., Weiss, A., 2012. An evaluation of MODIS 8-and 16-day composite products for monitoring maize green leaf area index. Agric. For. Meteorol. 161, 15–25.

Guo, X., Cui, P., Li, Y., Ma, L., Ge, Y., Mahoney, W.B., 2016. Intensity-duration threshold of rainfall-triggered debris flows in the Wenchuan Earthquake affected area, China. Geomorphology 253, 208–216. https://doi.org/10.1016/j.geomorph.2015.10.009.

Guthrie, R.H., Evans, S.G., 2004. Magnitude and frequency of landslides triggered by a storm event, Loughborough Inlet, British Columbia. Nat. Hazards Earth Syst. Sci. 4, 475–483.

Guzzetti, F., Malamud, B.D., Turcotte, D.L., Reichenbach, P., 2002. Power-law correlations of landslide areas in central Italy. Earth Planet. Sci. Lett. 195, 169–183.

Hovius, N., Stark, C.P., Allen, P.A., 1997. Sediment flux from a mountain belt derived by landslide mapping. Geology 25, 231–234.

Hovius, N., Meunier, P., Lin, C.W., Chen, H., Chen, Y.G., Dadson, S., Horng, M.J., Lines, M., 2011. Prolonged seismically induced erosion and the mass balance of a large earthquake. Earth Planet. Sci. Lett. https://doi.org/10.1016/j.epsl.2011.02.005.

Huang, F., Cao, Z., Guo, J., Jiang, S.H., Li, S., Guo, Z., 2020a. Comparisons of heuristic, general statistical and machine learning models for landslide susceptibility prediction and mapping. Catena 191, 104580. https://doi.org/10.1016/j.catena.2020.104580.

Huang, F., Cao, Z., Jiang, S.H., Zhou, C., Huang, J., Guo, Z., 2020b. Landslide susceptibility prediction based on a semi-supervised multiple-layer perceptron model. Landslides 17, 2919–2930. https://doi.org/10.1007/s10346-020-01473-9.

Huang, R., Fan, X., 2013. The landslide story. Nat. Geosci. https://doi.org/10.1038/ngeo1806.

Huang, R., Li, W., 2014. Post-earthquake landsliding and long-term impacts in the Wenchuan earthquake area. China. Eng. Geol. 182, 111–120. https://doi.org/10.1016/j.enggeo.2014.07.008.

Huyck, C., Scawthorn, C., Bardet, J.-P., Kayen, R., Kawamata, Y., Olshansky, R., Somerville, P., Mori, J., Rathje, E., Bay, J., 2005. Preliminary observations on the Niigata Ken Chuetsu, Japan, Earthquake of October 23, 2004. EERI Newsl. 39.

Japan Meteorological Agency, 2004. Press release materials (28th report on November10).

Jiang, S.H., Huang, J., Huang, F., Yang, J., Yao, C., Zhou, C.B., 2018. Modelling of spatial variability of soil undrained shear strength by conditional random fields for slope reliability analysis. Appl. Math. Model. 63, 374–389. https://doi.org/10.1016/j.apm.2018.06.030.

Justice, C.O., Townshend, J.R.G., Holben, B.N., Tucker, C.J., 1985. Analysis of the phenology of global vegetation using meteorological satellite data. Int. J. Remote Sens. 6, 1271–1318. https://doi.org/10.1080/01431168508948281.

Kato, A., Kurashimo, E., Hirata, N., Sakai, S., Iwasaki, T., 2005. Imaging the source region of the 2004 mid-Niigata prefecture earthquake and the evolution of a seismogenic thrust-related fold 32, 1–4. doi: 10.1029/2005GL022366.
Kato, A., Sakai, S., Hirata, N., Kurashimo, E., Iidaka, T., Iwasaki, T., Kanazawa, T., 2006. Imaging the seismic structure and stress field in the source region of the 2004 mid-Niigata prefecture earthquake: Structural zones of weakness and seismogenic stress concentration by ductile flow 111, 1–18. doi: 10.1029/2005JB004016.
Keefer, D.K., 1994. The importance of earthquake-induced landslides to long-term slope erosion and slope-failure hazards in seismically active regions. In: Geomorphology and Natural Hazards. Elsevier, pp. 265–284. doi: 10.1016/B978-0-444-82012-9.50022-0.
Khan, S.F., Kamp, U., Owen, L.A., 2013. Documenting five years of landsliding after the 2005 Kashmir earthquake, using repeat photography. Geomorphology 197, 45–55. https://doi.org/10.1016/j.geomorph.2013.04.033.
Larsen, I.J., Montgomery, D.R., 2012. Landslide erosion coupled to tectonics and river incision. Nat. Geosci. 5, 468–473.
Lei, J., Ren, Z., Oguchi, T., Zhang, P., Uchiyama, S., 2021. Topographic evolution involving co-seismic landslide, deformation, long-term folding and isostatic rebound: a case study on the 2004 Chuetsu earthquake. Remote Sens. 13, 1073.
Li, C., Wang, M., Liu, K., Xie, J., 2018. Topographic changes and their driving factors after 2008 Wenchuan earthquake. Geomorphology 311, 27–36. https://doi.org/10.1016/j.geomorph.2018.03.019.
Li, L., Yao, X., Zhang, Y., Iqbal, J., Chen, J., Zhou, N., 2016. Surface recovery of landslides triggered by 2008 Ms8. 0 Wenchuan earthquake (China): a case study in a typical mountainous watershed. Landslides 13, 787–794.
Lin, G.-W., Chen, H., Hovius, N., Horng, M.-J., Dadson, S., Meunier, P., Lines, M., 2008. Effects of earthquake and cyclone sequencing on landsliding and fluvial sediment transfer in a mountain catchment. Earth Surf. Process. Landforms J. Br. Geomorphol. Res. Gr. 33, 1354–1373.
Lin, W.T., Chou, W.C., Lin, C.Y., Huang, P.H., Tsai, J.S., 2005. Vegetation recovery monitoring and assessment at landslides caused by earthquake in Central Taiwan. For. Ecol. Manage. 210, 55–66. https://doi.org/10.1016/j.foreco.2005.02.026.
Lin, C.-W., Liu, S.-H., Lee, S.-Y., Liu, C.-C., 2006. Impacts of the Chi-Chi earthquake on subsequent rainfall-induced landslides in central Taiwan. Eng. Geol. 86, 87–101.
Lin, C.Y., Lo, H.M., Chou, W.C., Lin, W.T., 2004. Vegetation recovery assessment at the Jou-Jou Mountain landslide area caused by the 921 Earthquake in Central Taiwan. Ecol. Modell. 176, 75–81. https://doi.org/10.1016/j.ecolmodel.2003.12.037.
Liu, Y., Wang, T., Cai, C., Li, Z., Cheng, D., 2014. Effects of vegetation on runoff generation, sediment yield and soil shear strength on road-side slopes under a simulation rainfall test in the Three Gorges Reservoir Area. China. Sci. Total Environ. 485, 93–102.
Liu, S.-H., Chang, W.-S., Lin, C.-W., 2009. Rainfall-induced landslides in Chenyulan River watershed, central Taiwan: an example illustrates the impact of Chi-Chi earthquake on subsequent rainfall induced landslide. In: EGU General Assembly Conference Abstracts. p. 7191.
Luo, W., Dou, J., Fu, Y., Wang, X., He, Y., Ma, H., Wang, R., Xing, K., 2022. A novel hybrid LMD–ETS–TCN approach for predicting landslide displacement based on GPS time series analysis. Remote Sens. 15, 229. https://doi.org/10.3390/rs15010229.
Maharjan, S., Gnyawali, K.R., Tannant, D.D., Xu, C., Lacroix, P., 2021. Rapid terrain assessment for earthquake-triggered landslide susceptibility with high-resolution DEM and critical acceleration. Front. Earth Sci. 9, 1–14. https://doi.org/10.3389/feart.2021.689303.
Malamud, B.D., Turcotte, D.L., Guzzetti, F., Reichenbach, P., 2004. Landslide inventories and their statistical properties. Earth Surf. Process. Landforms 29, 687–711.
Maruyama, T., Fusejima, Y., Yoshioka, T., Awata, Y., Matsu'ura, T., 2005. Characteristics of the surface rupture associated with the 2004 Mid Niigata Prefecture earthquake, central Japan and their seismotectonic implications. Earth, planets Sp. 57, 521–526.
Matsushita, B., Yang, W., Chen, J., Onda, Y., Qiu, G., 2007. Sensitivity of the enhanced vegetation index (EVI) and normalized difference vegetation index (NDVI) to topographic effects: a case study in high-density cypress forest. Sensors 7, 2636–2651.
McPhillips, D., Bierman, P.R., Rood, D.H., 2014. Millennial-scale record of landslides in the Andes consistent with earthquake trigger. Nat. Geosci. 7, 925–930. https://doi.org/10.1038/ngeo2278.
Mondini, A.C., Guzzetti, F., Reichenbach, P., Rossi, M., Cardinali, M., Ardizzone, F., 2011. Semi-automatic recognition and mapping of rainfall induced shallow landslides using optical satellite images. Remote Sens. Environ. 115, 1743–1757. https://doi.org/10.1016/j.rse.2011.03.006.
Nakamura, H., Tsuchiya, S., Inoue, K., Ishikawa, Y., 2000. Sabo against earthquakes. Kokon Shoin, Tokyo 190, 220.
Niigata Prefectural Government, 2009. Niigata prefecture report on damage in the 2004 Niigata-Chuetsu earthquake (No. 174, final report). Niigata.
Okamura, Y., Ishiyama, T., Yanagisawa, Y., 2007. Fault-related folds above the source fault of the 2004 mid-Niigata Prefecture earthquake, in a fold-and-thrust belt caused by basin inversion along the eastern margin of the Japan Sea 112, 1–14. doi: 10.1029/2006JB004320.
Ouimet, W.B., 2010. Landslides associated with the May 12, 2008 Wenchuan earthquake: implications for the erosion and tectonic evolution of the Longmen Shan. Tectonophysics 491, 244–252. https://doi.org/10.1016/j.tecto.2009.09.012.
Oyagi, N., Uchiyama, S., Inokuchi, T., 2008. Map of landslides caused by the 2004 Niigata-ken Chuetsu (Mid Niigata) earthquake (MJMA= 6.8). Tech. Note Natl Res. Inst. Earth Sci. Disaster Prev. 317, 1–37.
Pandey, H.P., Gnyawali, K., Dahal, K., Pokhrel, N.P., Maraseni, T.N., 2022. Vegetation loss and recovery analysis from the 2015 Gorkha earthquake (7.8 Mw) triggered landslides. Land Use Policy 119. https://doi.org/10.1016/j.landusepol.2022.106185.
Parker, R.N., Densmore, A.L., Rosser, N.J., De Michele, M., Li, Y., Huang, R., Whadcoat, S., Petley, D.N., 2011. Mass wasting triggered by the 2008 Wenchuan earthquake is greater than orogenic growth. Nat. Geosci. 4, 449–452. https://doi.org/10.1038/ngeo1154.
Ren, Z., Zhang, Z., Dai, F., Yin, J., Zhang, H., 2014. Topographic changes due to the 2008 Mw7.9 Wenchuan earthquake as revealed by the differential DEM method. Geomorphology 217, 122–130. https://doi.org/10.1016/j.geomorph.2014.04.020.
Roback, K., Clark, M.K., West, A.J., Zekkos, D., Li, G., Gallen, S.F., Chamlagain, D., Godt, J.W., 2018. The size, distribution, and mobility of landslides caused by the 2015 Mw7. 8 Gorkha earthquake. Nepal. Geomorphol. 301, 121–138.
Roering, J., 2012. Landslides limit mountain relief. Nat. Geosci. 5, 446–447.
Rouse, J., Haas, R., Schell, J., Deering, D., 1974. Monitoring Vegetation Systems in the Great Plains with Erts. NASA Special Publication.
Rumpf, S.B., Hülber, K., Klonner, G., Moser, D., Schütz, M., Wessely, J., Willner, W., Zimmermann, N.E., Dullinger, S., 2018. Range dynamics of mountain plants decrease with elevation. Proc. Natl. Acad. Sci. 115, 1848–1853.
Saba, S.B., van der Meijde, M., van der Werff, H., 2010. Spatiotemporal landslide detection for the 2005 Kashmir earthquake region. Geomorphology 124, 17–25. https://doi.org/10.1016/j.geomorph.2010.07.026.
Saito, H., Uchiyama, S., Teshirogi, K., 2022. Rapid vegetation recovery at landslide scars detected by multitemporal high-resolution satellite imagery at Aso volcano. Japan. Geomorphology 398, 107989. https://doi.org/10.1016/j.geomorph.2021.107989.
Shafique, M., 2020. Spatial and temporal evolution of co-seismic landslides after the 2005 Kashmir earthquake. Geomorphology 362. https://doi.org/10.1016/j.geomorph.2020.107228.
Shao, X., Ma, S., Xu, C., 2022. Distribution and characteristics of shallow landslides triggered by the 2018 Mw 7.5 Palu earthquake, Indonesia. Landslides. https://doi.org/10.1007/s10346-022-01972-x.
Shen, P., Zhang, L.M., Chen, H.X., Gao, L., 2017. Role of vegetation restoration in mitigating hillslope erosion and debris flows. Eng. Geol. 216, 122–133.
Shen, P., Zhang, L.M., Fan, R.L., Zhu, H., Zhang, S., 2020. Declining geohazard activity with vegetation recovery during first ten years after the 2008 Wenchuan earthquake. Geomorphology 352, 106989. https://doi.org/10.1016/j.geomorph.2019.106989.
Shiels, A.B., West, C.A., Weiss, L., Klawinski, P.D., Walker, L.R., 2008. Soil factors predict initial plant colonization on Puerto Rican landslides. Plant Ecol. 195, 165–178.
Shou, K.J., Hong, C.Y., Wu, C.C., Hsu, H.Y., Fei, L.Y., Lee, J.F., Wei, C.Y., 2011a. Spatial and temporal analysis of landslides in Central Taiwan after 1999 Chi-Chi earthquake. Eng. Geol. 123, 122–128.
Shou, K.J., Wu, C.C., Fei, L.Y., Lee, J.F., Wei, C.Y., 2011b. Dynamic environment in the Ta-Chia River watershed after the 1999 Taiwan Chi-Chi earthquake. Geomorphology 133, 190–198. https://doi.org/10.1016/j.geomorph.2011.04.038.
Sidle, R.C., Bogaard, T.A., 2016. Dynamic earth system and ecological controls of rainfall-initiated landslides. Earth-science Rev. 159, 275–291.
Sidle, R.C., Ochiai, H., 2006. Landslides: Processes, Prediction, and Land Use. Wiley Online Library.
Stark, C.P., Hovius, N., 2001. The characterization of landslide size distributions. Geophys. Res. Lett. 28, 1091–1094.
Stokes, A., Atger, C., Bengough, A.G., Fourcaud, T., Sidle, R.C., 2009. Desirable plant root traits for protecting natural and engineered slopes against landslides. Plant Soil 324, 1–30.
Stumpf, A., Malet, J.P., Allemand, P., Ulrich, P., 2014. Surface reconstruction and landslide displacement measurements with Pléiades satellite images. ISPRS J. Photogramm. Remote Sens. 95, 1–12. https://doi.org/10.1016/j.isprsjprs.2014.05.008.
Sugai, T., Ohmori, H., Hirano, M., 1995. Rock control on magnitude-frequency distribution of landslide. In: International Journal of Rock Mechanics and Mining Sciences and Geomechanics Abstracts. p. 116A.
Geological Survey of Japan (Ed.), 2003. Geological maps of Japan 1:200,000.
Swanson, F.J., Dyrness, C.T., 1975. Impact of clear-cutting and road construction on soil erosion by landslides in the western Cascade Range, Oregon. Geology 3, 393–396.
Tang, H., Li, C., Hu, X., Su, A., Wang, L., Wu, Y., Criss, R., Xiong, C., Li, Y., 2015. Evolution characteristics of the Huangtupo landslide based on in situ tunneling and monitoring. Landslides 12, 511–521. https://doi.org/10.1007/s10346-014-0500-2.
Tang, H., Wasowski, J., Juang, C.H., 2019. Geohazards in the three Gorges Reservoir Area, China – lessons learned from decades of research. Eng. Geol. 261, 105267 https://doi.org/10.1016/j.enggeo.2019.105267.
Testa, S., Mondino, E.C.B., Pedroli, C., 2014. Correcting MODIS 16-day composite NDVI time-series with actual acquisition dates. Eur. J. Remote Sens. 47, 285–305. https://doi.org/10.5721/EuJRS20144718.
Valagussa, A., Marc, O., Frattini, P., Crosta, G.B., 2019. Seismic and geological controls on earthquake-induced landslide size. Earth Planet. Sci. Lett. 506, 268–281. https://doi.org/10.1016/j.epsl.2018.11.005.
Van Den Eeckhaut, M., Poesen, J., Govers, G., Verstraeten, G., Demoulin, A., 2007. Characteristics of the size distribution of recent and historical landslides in a populated hilly region. Earth Planet. Sci. Lett. 256, 588–603.
Wang, H.B., Sassa, K., Xu, W.Y., 2007. Analysis of a spatial distribution of landslides triggered by the 2004 Chuetsu earthquakes of Niigata Prefecture, Japan. Nat. Hazards. doi: 10.1007/s11069-006-9009-x.
Wang, J., Schweizer, D., Liu, Q., Su, A., Hu, X., Blum, P., 2021. Three-dimensional landslide evolution model at the Yangtze River. Eng. Geol. 292, 106275. doi: 10.1016/j.enggeo.2021.106275.
Wang, M., Yang, W., Shi, P., Xu, C., Liu, L., 2014. Diagnosis of vegetation recovery in mountainous regions after the wenchuan earthquake. IEEE J Sel. Top. Appl. Earth Obs. Remote Sens. 7, 3029–3037. https://doi.org/10.1109/JSTARS.2014.2327794.
Xiong, J., Tang, C., Tang, H., Chen, M., Zhang, X., Shi, Q., Chang, M., Gong, L., Li, N., Li, M., 2022. Long-term hillslope erosion and landslide–channel coupling in the area

of the catastrophic Wenchuan earthquake. Eng. Geol. 305, 106727 https://doi.org/10.1016/j.enggeo.2022.106727.
Xu, C., Xu, X., Shen, L., Yao, Q., Tan, X., Kang, W., Ma, S., Wu, X., Cai, J., Gao, M., et al., 2016. Optimized volume models of earthquake-triggered landslides. Sci. Rep. 6, 1–9.
Yang, W., Qi, W., Wang, M., Zhang, J., Zhang, Y., 2017. Spatial and temporal analyses of post-seismic landslide changes near the epicentre of the Wenchuan earthquake. Geomorphology 276, 8–15. https://doi.org/10.1016/j.geomorph.2016.10.010.
Yang, W., Qi, W., Zhou, J., 2018. Decreased post-seismic landslides linked to vegetation recovery after the 2008 Wenchuan earthquake. Ecol. Indic. 89, 438–444. https://doi.org/10.1016/j.ecolind.2017.12.006.
Yunus, A.P., Fan, X., Tang, X., Jie, D., Xu, Q., Huang, R., 2020. Decadal vegetation succession from MODIS reveals the spatio-temporal evolution of post-seismic landsliding after the 2008 Wenchuan earthquake. Remote Sens. Environ. 236, 111476 https://doi.org/10.1016/j.rse.2019.111476.
Zhang, G., Cui, P., Gualtieri, C., Zhang, J., Ahmed Bazai, N., Zhang, Z., Wang, J., Tang, J., Chen, R., Lei, M., 2021. Stormflow generation in a humid forest watershed controlled by antecedent wetness and rainfall amounts. J. Hydrol. 603, 127107 https://doi.org/10.1016/j.jhydrol.2021.127107.
Zhang, W., Xu, Y., Guo, X., Li, W., Du, P., Tian, Q., 2022. Distribution and characteristics of damming landslides triggered by 1920 M~8 Haiyuan earthquake. NW China. Remote Sens. 14 https://doi.org/10.3390/rs14102427.
Zhao, B., Wang, Y. sheng, Su, L. jun, Luo, Y. hong, Zhang, J., 2020b. Directional seismic response to the complex topography: a case study of 2013 Lushan Ms 7.0 earthquake. J. Mt. Sci. 17, 2049–2067. doi: 10.1007/s11629-020-6038-y.
Zhao, B., Wang, Y., Feng, Q., Guo, F., Zhao, X., Ji, F., Liu, J., Ming, W., 2020a. Preliminary analysis of some characteristics of coseismic landslides induced by the Hokkaido Iburi-Tobu earthquake (September 5, 2018), Japan. Catena 189, 104502. https://doi.org/10.1016/j.catena.2020.104502.
Zhao, B., Liao, H., Su, L., 2021. Landslides triggered by the 2018 Lombok earthquake sequence, Indonesia. Catena 207, 105676. https://doi.org/10.1016/j.catena.2021.105676.
Zhong, C., Li, C., Gao, P., Li, H., 2021. Discovering vegetation recovery and landslide activities in the wenchuan earthquake area with landsat imagery. Sensors 21, 1–16. https://doi.org/10.3390/s21155243.
Zhou, Y., Elliott, J.R., Parsons, B., Walker, R.T., 2015. The 2013 Balochistan earthquake: an extraordinary or completely ordinary event? Geophys. Res. Lett. 42, 6236–6243. https://doi.org/10.1002/2015GL065096.
Zhu, H., Zhang, L., 2019. Root-soil-water hydrological interaction and its impact on slope stability. Georisk Assess Manag. Risk Eng. Syst. Geohazards 13, 349–359.
Zou, Z., Yan, J., Tang, H., Wang, S., Xiong, C., Hu, X., 2020. A shear constitutive model for describing the full process of the deformation and failure of slip zone soil. Eng. Geol. 276, 105766 https://doi.org/10.1016/j.enggeo.2020.105766.